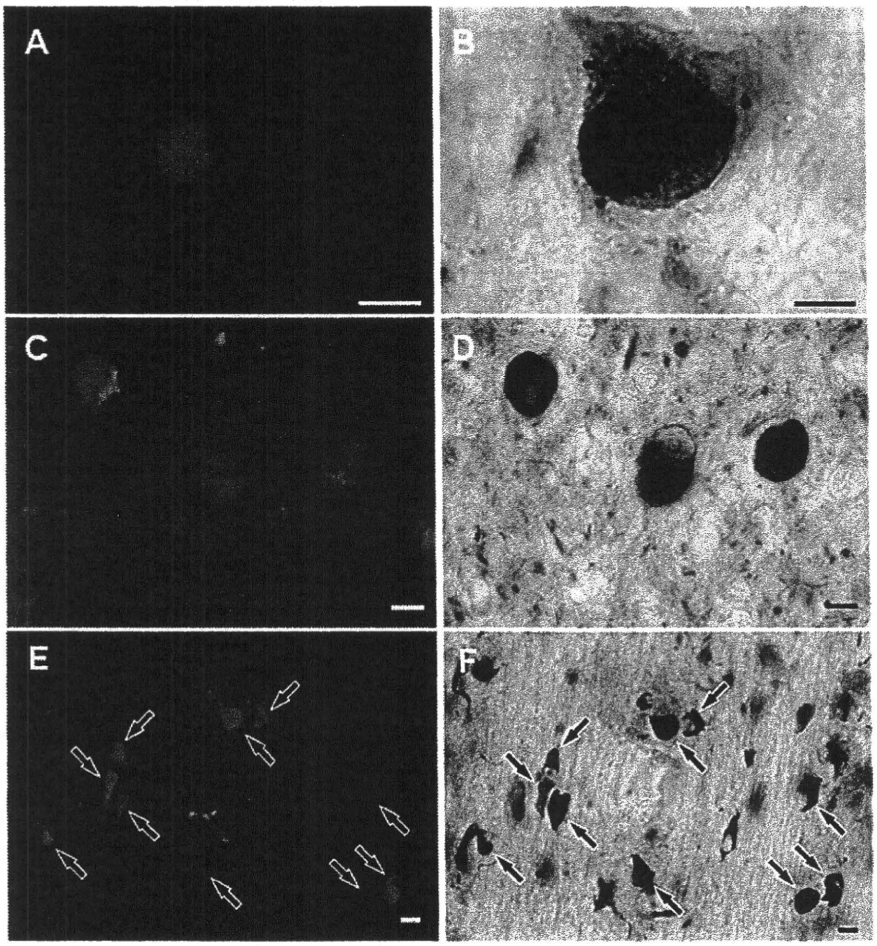

Figure 1 Neuropathological findings of BF-227 fluorostaining and anti-phosphorylated α-synuclein antibody immunostaining. BF-227 fluorostaining (**A** and **C**) and anti-phosphorylated α-synuclein antibody immunostaining (**B** and **D**) showed colocalization of these proteins in brainstem-type Lewy bodies in the substantia nigra of patients with Parkinson's disease (**A** and **B**) and in cortical Lewy bodies in the temporal lobe of patients dementia with Lewy bodies (**C** and **D**). Similarly, BF-227 fluorostaining (**E**) and anti-phosphorylated α-synuclein antibody immunostaining (**F**) were codetected in glial cytoplasmic inclusions in the pontine base of a patient with MSA. BF-227 histofluorescence was observed in the most of glial cytoplasmic inclusions (arrows). Bars = 10 μm.

(uncorrected $P<0.005$), globus pallidus, primary motor cortex and anterior cingulate cortex (uncorrected $P<0.01$) and substantia nigra (uncorrected $P<0.05$) in patients with MSA compared to the normal controls (Table 2 and Fig. 2D). It is noteworthy that the distribution volume of [^{11}C]-BF-227 was significantly high in the subcortical white matter even if Bonferroni's multiple comparison test was applied. On the other hand, no obvious differences were found in either the distribution or degree of binding between the MSA with predominant parkinsonism and MSA with predominant cerebellar ataxia subgroups.

Discussion

The BF-227 stained α-synuclein-containing Lewy bodies (Fig. 1A–D) and glial cytoplasmic inclusions (Fig. 1E and F) in formalin-fixed tissue sections as well as β-amyloid-containing senile plaques in paraffin-embedded tissue sections (Kudo *et al.*, 2007). These results were consistent with the previous findings showing BF-227 binding to synthetic α-synuclein fibrils with high affinity (K_d 9.63 nM) (Fodero-Tavoletti *et al.*, 2009), and to Lewy bodies in paraffin-embedded tissue sections (Fodero-Tavoletti *et al.*, 2009).

The anti-phosphorylated α-synuclein antibody immunostained the halo region more intensively compared with the central core in Lewy bodies in the substantia nigra of Parkinson's disease, while the BF-227 staining was intensely observed in the core of Lewy bodies (Fig. 1A and B). Because intense thioflavin S staining was also reported in the core of nigral Lewy bodies (Duda *et al.*, 2000), the core is thought to be rich in β-sheet structures. Similar to thioflavin S, the BF-227 staining is considered to recognize amyloid-like β-pleated sheets, and it was suggested to be the reason for the more intense BF-227 staining in the core of Lewy bodies. In addition, the high density of the core structure

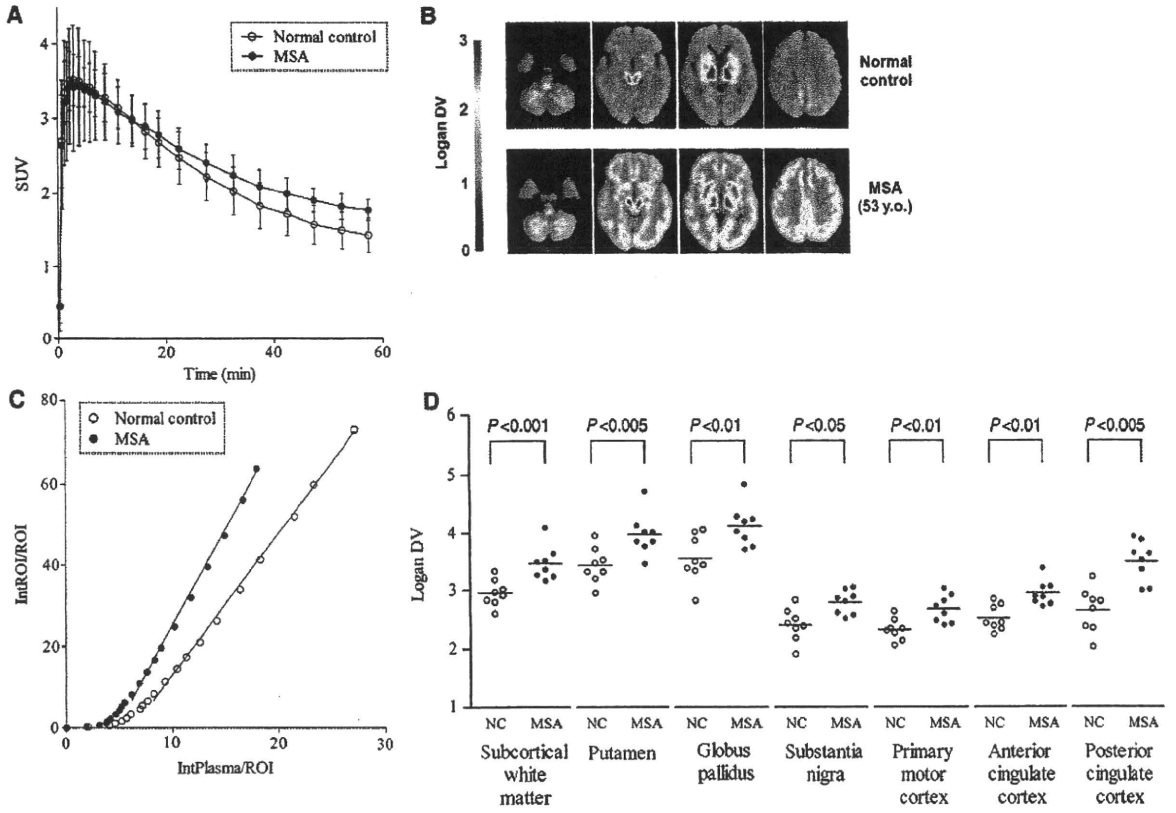

Figure 2 [^{11}C]-BF-227 PET findings in MSA. Time activity curves showed initial rapid uptake of radioactivity followed by gradual clearance in the putamen of both normal subjects and MSA cases. Data are mean ± SD of eight normal subjects and eight patients with MSA (**A**). In a representative patient with MSA with predominant cerebellar ataxia, the regional distribution volumes were mapped to the subcortical white matter and lentiform nucleus compared to normal control (**B**). Typical Logan plots for the putamen were presented in a representative patient with MSA with predominant cerebellar ataxia and a normal control. The slopes of the linear regression curves on Logan plot analysis represent the distribution volume of the tracer in the putamen (**C**). There were differences in the mean regional distribution volume values between patients with MSA and normal control in the subcortical white matter (uncorrected $P<0.001$), putamen and posterior cingulate cortex (uncorrected $P<0.005$), globus pallidus, primary motor cortex and anterior cingulate cortex (uncorrected $P<0.01$) and substantia nigra (uncorrected $P<0.05$). Data of individual subjects (symbols) and mean values (horizontal lines) (**D**). SUV = standardized uptake value; DV = distribution volume; ROI = region of interest.

may often prevent the penetration of antibodies into this region (Galloway *et al.*, 1992), since electron microscopic studies revealed that vesicular structures were tightly packed in the core of Lewy bodies (Takahashi and Wakabayashi, 2005). On the other hand, not all glial cytoplasmic inclusions stained by anti-phosphorylated α-synuclein antibody were always positive for BF-227 staining (Fig. 1E and F). In the process of oligodendroglial pathology, it was believed that α-synuclein deposits as amorphous state and then forms fibrillar structures (Gai *et al.*, 2003; Stefanova *et al.*, 2005). In fact, part of glial cytoplasmic inclusions were reported to be α-synuclein-negative (Sakamoto *et al.*, 2005) and therefore, it seems reasonable that some of glial cytoplasmic inclusions were not composed of β-sheet fibrils and were negative for BF-227 staining.

The regional distribution volume of [^{11}C]-BF-227 was the highest in the subcortical white matter, followed by the putamen, posterior cingulate cortex, anterior cingulate cortex, globus pallidus, primary motor cortex and substantia nigra, in which glial cytoplasmic inclusions were densely distributed (Papp and Lantos, 1994; Inoue *et al.*, 1997; Wakabayashi and Takahashi, 2006) and large increases of α-synuclein content were found (Tong *et al.*, 2010) in the post-mortem brains. Thus, it was suggested that the distributions of [^{11}C]-BF-227 could properly reflect those of the α-synuclein deposits *in vivo*. On the other hand, the regional distribution volume in other affected brain regions, such as the cerebellum and pons (Ozawa *et al.*, 2004; Wakabayashi and Takahashi, 2006), did not show higher values relative to the normal control group. The glial cytoplasmic inclusions in cerebellum were reported to decrease along with the disease progression and concomitant neuronal loss (Inoue *et al.*, 1997). Therefore, it is plausible that the accumulation levels of glial cytoplasmic inclusions are changing and do not always increase with the disease progression (Mochizuki *et al.*, 1992; Inoue *et al.*, 1997). Moreover, due to the remarkable cerebellar and pontine atrophy,

Table 2 Distribution volume of [11C]BF-227

	Normal controls	MSA
Frontal cortex	2.28±0.18	2.46±0.22
Primary motor cortex	2.40±0.28	2.79±0.20¶
Parietal cortex	2.48±0.26	2.63±0.24
Medial temporal cortex	2.44±0.21	2.82±0.31
Lateral temporal cortex	2.42±0.19	2.63±0.23
Occipital cortex	2.43±0.20	2.72±0.27
Anterior cingulate cortex	2.32±0.18	2.67±0.23¶
Posterior cingulate cortex	2.52±0.22	2.94±0.22†
Subcortical white matter	2.65±0.38	3.49±0.36‡
Caudate nucleus	2.70±0.21	3.05±0.34
Putamen	2.95±0.23	3.47±0.30†
Globus pallidus	3.43±0.31	3.97±0.36¶
Thalamus	3.50±0.28	4.03±0.31
Substantia nigra	3.55±0.41	4.12±0.36*
Midbrain tegmentum	3.53±0.54	3.45±0.47
Pons	3.63±0.54	3.88±0.42
Cerebellar cortex	2.32±0.22	2.16±0.29

Data are mean ± SD.
*Uncorrected $P<0.05$.
¶Uncorrected $P<0.01$.
†Uncorrected $P<0.005$.
‡Uncorrected $P<0.001$.

the distribution volume in these regions might be underestimated. Correction for partial volume loss is therefore needed to improve the accuracy of quantification in the cerebellum and brainstem of MSA. BF-227 fluorescent signal was detected in β-amyloid plaques as well as glial cytoplasmic inclusions and Lewy bodies (Fig. 1A–F) in neuropathological staining (Kudo *et al.*, 2007). However, the differences in the distribution of [11C]-BF-227 by PET could discriminate MSA from Alzheimer's disease, which showed high distribution of [11C]-BF-227 in the temporoparietal–occipital region (Kudo *et al.*, 2007). In our preliminary studies, Parkinson's disease and dementia with Lewy bodies also showed quite different patterns of distribution volumes from those of MSA (data not shown). Therefore, MSA could be distinguished from other degenerative diseases such as Alzheimer's disease, Parkinson's disease and dementia with Lewy bodies by the [11C]-BF-227 PET.

The affinity of BF-227 to α-synuclein fibrils (K_d 9.63 nM) was reported to be almost identical to that of PIB (K_d 10.07 nM) (Fodero-Tavoletti *et al.*, 2007, 2009). However, in the post-mortem human brain, the PIB binding was not colocalized with α-synuclein-positive Lewy bodies in two reports (Fodero-Tavoletti *et al.*, 2007; Ye *et al.*, 2008) although one report showed PIB binding to Lewy bodies in the substantia nigra of Parkinson's disease (Maetzler *et al.*, 2008). Therefore, there is controversy as to whether PIB binds to α-synuclein-containing Lewy bodies. Moreover, there have been no reports showing that PIB could detect α-synuclein deposits in α-synucleinopathies by PET (Fodero-Tavoletti *et al.*, 2007; Johansson *et al.*, 2008; Maetzler *et al.*, 2008). The hydroxy group in PIB (Mathis *et al.*, 2003) may prevent it from passing through the cell membranes and thereby detecting α-synuclein depositions in the cytoplasm, however, the BF-227 is more lipophilic than PIB (Mathis *et al.*, 2003), and may easily pass into the cytoplasm and bind to α-synuclein aggregates. As shown in the present study, BF-227 is a promising tracer to detect glial cytoplasmic inclusions. Further studies are warranted to verify whether Lewy bodies in other α-synucleinopathies as well as glial cytoplasmic inclusions can be detected by [11C]-BF-227 PET.

In conclusion, the BF-227 could bind to α-synuclein-containing glial cytoplasmic inclusions (Fig. 1E and F) in the post-mortem brain, and the [11C]-BF-227 PET demonstrated high signals in the glial cytoplasmic inclusion-rich brain regions including subcortical white matter, putamen, globus pallidus, primary motor cortex and anterior and posterior cingulate cortex (Table 2 and Fig. 2D). These results suggest that [11C]-BF-227 PET is a suitable surrogate maker for monitoring α-synuclein deposits in living brains with MSA and could be a potential tool to monitor the effectiveness of neuroprotective therapy for α-synucleinopathies.

Funding

Grant for 'the Research Committee for Ataxic Diseases' of the Research on Measures for Intractable Diseases from the Ministry of Health, Labour and Welfare, Japan (partial).

References

Dejerine J, Thomas A. L'atrophie olivo-ponto-cérébelleuse. Nouvelle Iconographie Salpêtrière 1900; 13: 330–7.

Duda JE, Lee VM, Trojanowski JQ. Neuropathology of synuclein aggregates. J Neurosci Res 2000; 61: 121–7.

Fodero-Tavoletti MT, Mulligan RS, Okamura N, Furumoto S, Rowe CC, Kudo Y, et al. In vitro characterisation of BF227 binding to alpha-synuclein/Lewy bodies. Eur J Pharmacol 2009; 617: 54–8.

Fodero-Tavoletti MT, Smith DP, McLean CA, Adlard PA, Barnham KJ, Foster LE, et al. In vitro characterization of Pittsburgh compound-B binding to Lewy bodies. J Neurosci 2007; 27: 10365–71.

Fujishiro H, Ahn TB, Frigerio R, DelleDonne A, Josephs KA, Parisi JE, et al. Glial cytoplasmic inclusions in neurologically normal elderly: prodromal multiple system atrophy? Acta Neuropathol 2008; 116: 269–75.

Gai WP, Pountney DL, Power JH, Li QX, Culvenor JG, McLean CA, et al. alpha-Synuclein fibrils constitute the central core of oligodendroglial inclusion filaments in multiple system atrophy. Exp Neurol 2003; 181: 68–78.

Galloway PG, Mulvihill P, Perry G. Filaments of Lewy bodies contain insoluble cytoskeletal elements. Am J Pathol 1992; 140: 809–22.

Gilman S, Low PA, Quinn N, Albanese A, Ben-Shlomo Y, Fowler CJ, et al. Consensus statement on the diagnosis of multiple system atrophy. J Neurol Sci 1999; 163: 94–8.

Gilman S, Wenning GK, Low PA, Brooks DJ, Mathias CJ, Trojanowski JQ, et al. Second consensus statement on the diagnosis of multiple system atrophy. Neurology 2008; 71: 670–6.

Hirohata M, Ono K, Morinaga A, Yamada M. Non-steroidal anti-inflammatory drugs have potent anti-fibrillogenic and fibril-destabilizing effects for alpha-synuclein fibrils in vitro. Neuropharmacology 2008; 54: 620–7.

Inoue M, Yagishita S, Ryo M, Hasegawa K, Amano N, Matsushita M. The distribution and dynamic density of oligodendroglial cytoplasmic inclusions (GCIs) in multiple system atrophy: a correlation between the density of GCIs and the degree of involvement of striatonigral and olivopontocerebellar systems. Acta Neuropathol 1997; 93: 585–91.

Iwata R, Pascali C, Bogni A, Miyake Y, Yanai K, Ido T. A simple loop method for the automated preparation of (11C)raclopride from (11C)methyl triflate. Appl Radiat Isot 2001; 55: 17–22.

Jewett DM. A simple synthesis of [11C]methyl triflate. Int J Rad Appl Instrum [A] 1992; 43: 1383–5.

Johansson A, Savitcheva I, Forsberg A, Engler H, Langstrom B, Nordberg A, et al. [(11)C]-PIB imaging in patients with Parkinson's disease: preliminary results. Parkinsonism Relat Disord 2008; 14: 345–7.

Kudo Y, Okamura N, Furumoto S, Tashiro M, Furukawa K, Maruyama M, et al. 2-(2-[2-Dimethylaminothiazol-5-yl]ethenyl)-6-(2-[fluoro]ethoxy)benzoxazole: a novel PET agent for in vivo detection of dense amyloid plaques in Alzheimer's disease patients. J Nucl Med 2007; 48: 553–61.

Logan J. Graphical analysis of PET data applied to reversible and irreversible tracers. Nucl Med Biol 2000; 27: 661–70.

Maetzler W, Reimold M, Liepelt I, Solbach C, Leyhe T, Schweitzer K, et al. [11C]PIB binding in Parkinson's disease dementia. Neuroimage 2008; 39: 1027–33.

Marti MJ, Tolosa E, Campdelacreu J. Clinical overview of the synucleinopathies. Mov Disord 2003; 18(Suppl): S21–7.

Mathis CA, Wang Y, Holt DP, Huang GF, Debnath ML, Klunk WE. Synthesis and evaluation of 11C-labeled 6-substituted 2-arylbenzothiazoles as amyloid imaging agents. J Med Chem 2003; 46: 2740–54.

Mochizuki A, Mizusawa H, Ohkoshi N, Yoshizawa K, Komatsuzaki Y, Inoue K, et al. Argentophilic intracytoplasmic inclusions in multiple system atrophy. J Neurol 1992; 239: 311–6.

Ono K, Yamada M. Antioxidant compounds have potent anti-fibrillogenic and fibril-destabilizing effects for alpha-synuclein fibrils in vitro. J Neurochem 2006; 97: 105–15.

Ozawa T, Paviour D, Quinn NP, Josephs KA, Sangha H, Kilford L, et al. The spectrum of pathological involvement of the striatonigral and olivopontocerebellar systems in multiple system atrophy: clinicopathological correlations. Brain 2004; 127: 2657–71.

Papp MI, Lantos PL. The distribution of oligodendroglial inclusions in multiple system atrophy and its relevance to clinical symptomatology. Brain 1994; 117(Pt 2): 235–43.

Sakamoto M, Uchihara T, Nakamura A, Mizutani T, Mizusawa H. Progressive accumulation of ubiquitin and disappearance of alpha-synuclein epitope in multiple system atrophy-associated glial cytoplasmic inclusions: triple fluorescence study combined with Gallyas-Braak method. Acta Neuropathol 2005; 110: 417–25.

Shy GM, Drager GA. A neurological syndrome associated with orthostatic hypotension: a clinical-pathologic study. Arch Neurol 1960; 2: 511–27.

Stefanova N, Reindl M, Neumann M, Haass C, Poewe W, Kahle PJ, et al. Oxidative stress in transgenic mice with oligodendroglial alpha-synuclein overexpression replicates the characteristic neuropathology of multiple system atrophy. Am J Pathol 2005; 166: 869–76.

Takahashi H, Wakabayashi K. Controversy: is Parkinson's disease a single disease entity? Yes. Parkinsonism Relat Disord 2005; 11(Suppl 1): S31–7.

Tashiro M, Okamura N, Furumoto S, Kumagai K, Furukawa K, Sugi K, et al. Quantitative analysis of amyloid deposition in Alzheimer's disease patients and healthy volunteers using PET and [11C]BF-227. In: Proceedings of the International Symposium on Early Detection and Rehabilitation Technology of Dementia 2009 (DRD2009). Okayama, Japan, 2009.110–1.

Tong J, Wong H, Guttman M, Ang LC, Forno LS, Shimadzu M, et al. Brain alpha-synuclein accumulation in multiple system atrophy, Parkinson's disease and progressive supranuclear palsy: a comparative investigation. Brain 2010; 133: 172–88.

van der Eecken H, Adams RD, van Bogaert L. Striopallidal-nigral degeneration. An hitherto undescribed lesion in paralysis agitans. J Neuropathol Exp Neurol 1960; 19: 159–61.

Wakabayashi K, Takahashi H. Cellular pathology in multiple system atrophy. Neuropathology 2006; 26: 338–45.

Wakabayashi K, Yoshimoto M, Tsuji S, Takahashi H. Alpha-synuclein immunoreactivity in glial cytoplasmic inclusions in multiple system atrophy. Neurosci Lett 1998; 249: 180–2.

Ye L, Velasco A, Fraser G, Beach TG, Sue L, Osredkar T, et al. In vitro high affinity alpha-synuclein binding sites for the amyloid imaging agent PIB are not matched by binding to Lewy bodies in postmortem human brain. J Neurochem 2008; 105: 1428–37.

Journal of Neurochemistry

JOURNAL OF NEUROCHEMISTRY | 2009 | 109 | 1648–1657 doi: 10.1111/j.1471-4159.2009.06069.x

A traditional medicinal herb *Paeonia suffruticosa* and its active constituent 1,2,3,4,6-penta-*O*-galloyl-β-D-glucopyranose have potent anti-aggregation effects on Alzheimer's amyloid β proteins *in vitro* and *in vivo*

Hironori Fujiwara,* Masahiro Tabuchi,† Takuji Yamaguchi,† Koh Iwasaki,* Katsutoshi Furukawa,‡ Kyoji Sekiguchi,† Yasushi Ikarashi,† Yukitsuka Kudo,§ Makoto Higuchi,¶,** Takaomi C. Saido,** Sumihiro Maeda,†† Akihiko Takashima,†† Masahiko Hara,‡‡ Nobuo Yaegashi,* Yoshio Kase† and Hiroyuki Arai‡

*Center for Asian Traditional Medicine, Tohoku University Graduate School of Medicine, Sendai, Aoba-ku, Japan

†TSUMURA Research Laboratories, TSUMURA & Co., Ibaraki, Japan

‡Department of Geriatrics and Gerontology, Division of Brain Sciences, Institute of Development, Aging and Cancer, Tohoku University, Aoba-ku, Sendai, Japan

§Innovation of Biomedical Engineering Center, Tohoku University, Aoba-ku, Sendai, Japan

¶Molecular Imaging Center, National Institute of Radiological Sciences, Inage-ku, Chiba, Japan

**Laboratory for Proteolytic Neuroscience, RIKEN Brain Science Institute, Wako, Saitama, Japan

††Laboratory for Alzheimer's Disease, RIKEN Brain Science Institute, Wako, Saitama, Japan

‡‡Local Spatio-Temporal Functions Laboratory, RIKEN Frontier Research System, Wako, Saitama, Japan

Abstract

The deposition of amyloid β (Aβ) protein is a consistent pathological hallmark of Alzheimer's disease (AD) brains; therefore, inhibition of Aβ fibril formation and destabilization of pre-formed Aβ fibrils is an attractive therapeutic and preventive strategy in the development of disease-modifying drugs for AD. This study demonstrated that *Paeonia suffruticosa*, a traditional medicinal herb, not only inhibited fibril formation of both $A\beta_{1-40}$ and $A\beta_{1-42}$ but it also destabilized pre-formed Aβ fibrils in a concentration-dependent manner. Memory function was examined using the passive-avoidance task followed by measurement of Aβ burden in the brains of Tg2576 transgenic mice. The herb improved long-term memory impairment in the transgenic mice and inhibited the accumulation of Aβ in the brain. Three-dimensional HPLC analysis revealed that a water extract of the herb contained several different chemical compounds including 1,2,3,4,6-penta-*O*-galloyl-β-D-glucopyranose (PGG). No obvious adverse/toxic were found following treatment with PGG. As was observed with *Paeonia suffruticosa*, PGG alone inhibited Aβ fibril formation and destabilized pre-formed Aβ fibrils *in vitro* and *in vivo*. Our results suggest that both *Paeonia suffruticosa* and its active constituent PGG have strong inhibitory effects on formation of Aβ fibrils *in vitro* and *in vivo*. PGG is likely to be a safe and promising lead compound in the development of disease-modifying drugs to prevent and/or cure AD.

Keywords: 1,2,3,4,6-penta-*O*-galloyl-β-D-glucopyranose, Alzheimer's disease, amyloid β protein, medicinal herb, *Paeonia suffruticosa*, Tg2576 transgenic mice.

J. Neurochem. (2009) **109**, 1648–1657.

Received November 27, 2008; revised manuscript received March 10, 2009; accepted March 23, 2009.

Address correspondence and reprint requests to Hiroyuki Arai, M.D., Ph.D., Department of Geriatrics and Gerontology, Division of Brain Sciences, Institute of Development, Aging and Cancer, Tohoku University, 4-1 Seiryo-cho Aobaku, Sendai 980-8575, Japan.
E-mail: harai@idac.tohoku.ac.jp

Abbreviations used: AD, Alzheimer's disease; APP, amyloid precursor protein; Aβ, amyloid β; MTT, 3-(4,5-dimethylthiazol-2-yl)-2,5-diphenyltetrazolium bromide; PGG, 1,2,3,4,6-penta-*O*-galloyl-β-D-glucopyranose.

Alzheimer's disease (AD) is the most prevalent cause of dementia and is characterized by loss of memory and cognition as well as behavioral and occupational instability in old age. One of the pathological characteristics of AD is the progressive deposition of insoluble amyloid β protein (Aβ) as a form of senile plaques (Wirths *et al.* 2004). This protein comprises peptides of approximately 39 to 43 amino acid residues derived from the transmembrane amyloid precursor protein (APP) (Selkoe 2002). Aβ can form monomers and a variety of different aggregate morphologies including dimers, small soluble oligomers, protofibrils, diffuse plaques, and fibrillar deposits seen in the senile plaques. Protofibrils, diffuse plaques, and fibrillar deposits seem to have a predominant β-sheet structure (Tierney *et al.* 1988; Barrow and Zagorski 1991), while oligomers are believed to be more globular (Barghorn *et al.* 2005). Increasing evidence that the formation of these aggregates, particularly oligomer, causes primary neurodegeneration in AD has led to the amyloid hypothesis which states that the accumulation of Aβ in the CNS is highly neurotoxic and deteriorates synaptic functions (Selkoe 2002; Wirths *et al.* 2004). Moreover, several lines of evidence suggest that Aβ accumulation begins at relatively early stages before cognitive decline becomes manifest (Anderton *et al.* 1998; Selkoe 2002). Therefore, it is hypothesized that the formation, deposition, and aggregation of Aβ in the brain should be primary targets for complete amelioration of dementia. Currently, drugs available for dementia such as acetylcholinesterase inhibitors exert only a temporary benefit on cognitive dysfunction (Millard and Broomfield 1995; Park *et al.* 2000; Darreh-Shori *et al.* 2004), and they do not prevent or reverse the formation of Aβ deposits. One potentially promising strategy for developing more effective anti-dementia drugs is the inhibition of Aβ fibril formation or destabilization of aggregated Aβ or a combination of both.

Herbal remedies are used worldwide and have a long history of use in alleviating a variety of symptoms of many different conditions and diseases. Recently, clinical trials in AD patients have also shown that some of these traditional medications improved Mini-Mental State Examination scores, P300 latency, and blood flow in the cerebral cortex (Le Bars *et al.* 1997). Although inconclusive, these provocative studies suggest that even old remedies can be beneficial in AD and related disorders. We have reported that several traditional herbal medicines such as *Formula lienalis angelicae compositae* (kamiuntanto) (Suzuki *et al.* 2001; Nakagawasai *et al.* 2004), *Pilulae octo-medicamentorum rehmanniae* (hachimijiogan) (Iwasaki *et al.* 2004), and *Pulvis depressionis hepatis* (yokukansan) (Iwasaki *et al.* 2005) improved symptoms of dementia. The radicis cortex of *Paeonia suffruticosa* (*Moutan cortex*; Botan-pi), a major medicinal plant comprising *Pilulae octo-medicamentorum rehmanniae*, is used as an anti-pyretic and anti-inflammatory agent (Lin *et al.* 1999; Yasuda *et al.* 1999; Chou 2003). Paeonol, a common component of *Paeonia suffruticosa*, has been shown to inhibit platelet aggregation in rabbits (Lin *et al.* 1999) as well as to reduce cerebral infarction in ischemia-reperfusion-injured rats (Hsieh *et al.* 2006). However, the underlying mechanism of traditional medicinal herbs, including *Paeonia suffruticosa*, on the formation and metabolism of Aβ fibrils has never been investigated. In the present study, we examined the effect of *Paeonia suffruticosa* on the formation of Aβ aggregates and its ability to destabilize pre-formed Aβ fibrils *in vitro* by using fluorescence spectroscopy with thioflavin T.

1,2,3,4,6-Penta-*O*-galloyl-β-D-glucopyranose (PGG), a high molecular weight tannin-type polyphenols, has been isolated from *Paeonia suffruticosa*. The defining characteristic of tannins is their ability to bind and precipitate proteins (Hofmann *et al.* 2006). Li *et al.* (2005) previously reported that PGG could bind to insulin receptors and activate an insulin-mediated glucose transport signaling pathway. However, the effect of this compound on the formation and metabolism of Aβ fibrils has not yet been investigated.

Our results provide strong evidence that several traditional herbs extracts including *Paeonia suffruticosa* and PGG have inhibitory and destabilizing effects on Aβ fibrils.

Materials and methods

Reagents

Aβ peptides (1–40 and 1–42) and thioflavin-T were obtained from Peptide Institute (Osaka, Japan) and from Sigma (St Louis, MO, USA), respectively. All the reagents and drugs used were of analytical grade.

Preparation of medicinal herb extracts

Water, 100% methanol, and 99.5% ethanol extracts of medicinal herbs were prepared by refluxing 10 g of sliced dry herbs in 100 mL of each solution for 30 min. The decoction after cooling to 25°C was evaporated completely under reduced pressure to yield dried or oily extracts. The extracts were weighed and dissolved in dimethylsulfoxide at a concentration of 100 mg/mL and then stored at −20°C. When assaying, these extracts were dissolved in 50 mM potassium phosphate buffer (pH 7.4) and the solutions were adjusted to pH 7.4 when necessary.

Analysis of three-dimensional HPLC fingerprints of water extract of *Paeonia suffruticosa*

Paeonia suffruticosa (0.5 g) was extracted with 30 mL of distilled water under ultrasonication for 30 min. The solution was filtered and then analyzed by HPLC. The HPLC system consisted of an HPLC pump (LC-10AD; Shimadzu, Kyoto, Japan) and a TSK-GEL 80_{TS} column (4.6 mm × 250 mm), and (A) 50 mM acetic acid-ammonium acetate and (B) acetonitrile were used as the eluents. A linear gradient of 90% A and 10% B changing over 60 min to 0% A and 100% B was used. The flow rate was controlled at 1.0 mL/min. After the eluate was obtained from the column, the three-dimensional data were processed with a diode array detector (SPD-M10A; Shimadzu).

Thioflavin-T measurement

Thioflavin-T measurement was performed using the method described by Suemoto *et al.* (2004) with slight modifications. For the Aβ aggregate-formation assay, Aβ (20 μM) dissolved in the 50 mM potassium phosphate buffer (pH 7.4) with a test herbal extract was incubated at 37°C for 96 h ($A\beta_{1-40}$) or 24 h ($A\beta_{1-42}$). For the destabilization assay of pre-formed Aβ aggregates, after incubation of $A\beta_{1-40}$ (96 h) or $A\beta_{1-42}$ (24 h) without a test herbal extract, a mixture of the aggregated Aβ and a test herbal extract was incubated for 30 min at 37°C.

At the end of the incubation, 3 μM thioflavin-T dissolved in 100 mM glycine buffer (pH 8.5) was added to the mixture. Fluorescence of thioflavin-T bound to Aβ aggregates was measured using a microplate reader (Spectramax GEMINI XS; Molecular Devices, Sunnyvale, CA, USA) (excitation at 442 nm and emission at 485 nm) after incubation for 30 min at 25°C. The percentage inhibition was calculated by comparing the fluorescence values of test samples with those of control solutions without herbal extracts.

Animals

Tg2576 APPswe mice over-express a 695-amino acid splice form (Swedish mutation K670N M671I) of the human Aβ precursor protein (APP695) which resulted in a fivefold increase in $A\beta_{1-40}$ and a 14-fold increase in $A\beta_{1-42}$ with increasing age, driven by the hamster prion protein promoter. The animals were allowed free access to water and standard laboratory food in a facility with the temperature controlled at 24 ± 1°C and relative humidity at 55 ± 5%, with lights on from 7:00 to 19:00 hours daily. Behavioral studies were performed between 10:00 and 12:00 hours. Experimental protocols were approved by the Animal Care and Use Committee, Tohoku University Graduate School of Medicine, and complied with the procedures outlined in the Guide for the Care and Use of Laboratory Animals of Tohoku University.

Step-through passive-avoidance test

The apparatus (AP model; O'Hara Co., Tokyo, Japan) for the step-through passive-avoidance test consisted of two compartments, illuminated compartment [100 mm × 120 mm × 100 mm; light at the top of compartment (27W, 3000 lx)] and dark compartment (100 mm × 170 mm × 100 mm). The compartments were separated by a guillotine door. During the learning stage, a mouse was placed in the illuminated safe compartment. As the compartment was lit, the mouse stepped through the opened guillotine door into the dark compartment. The time spent in the illuminated compartment was defined as the latency time. Three seconds after the mouse entered the dark compartment, a foot shock (0.3 mA, 50V, 50 Hz ac, for 3 s) was delivered to the floor grids in the dark compartment. The mouse could escape from the shock only by stepping back to the safe illuminated compartment. Such acquisition trials during the learning stage were carried out once a day for 5 days. It was judged as learning avoidance from foot-shock if the mouse remained in the illuminated compartment for 300 s after being placed there. The retention trials were carried out once per week for 10 weeks from Days 8 to 78 to evaluate the retention of avoidance memory. The latency time was measured for up to 300 s without delivering foot-shock. It was judged that the mouse retained the avoidance memory when it stayed in the illuminated safe compartment for 300 s. Acquisition and retention trials were conducted in 11-month-old mice.

Immunocytochemistry

All sample brains were fixed in neutral-buffered formalin and embedded in paraffin. Immunocytochemistry was performed using an Amyloid β Protein Immunohistostain Kit (Wako Pure Chemical Industries, Ltd., Osaka, Japan) according to the manufacturer's instructions. Briefly, after deparaffinization, 8-μm brain sections were immersed in 99% formic acid for 5 min, blocked with blocking serum, and immunostained with BA27 ($A\beta_{1-40}$) and BC05 ($A\beta_{1-42}$) by a standard avidin–biotin complex method, using 3,3′-diaminobenzidine as chromogen and lightly counter-staining with hematoxylin.

Tissue preparation

Tissue samples were processed in Tris-buffered saline (soluble fraction) and 70% formic acid (insoluble fraction) containing 1× protease inhibitor mixtures as described previously (Calon *et al.* 2004) with slight modifications. Briefly, brain tissues were homogenized and sonicated in Tris-buffered saline containing protease inhibitor mixture. The resulting homogenate was subjected to ultracentrifugation at 200 000 *g* at 4°C for 20 min, and the soluble supernatant was collected and frozen. To analyze the insoluble Aβ, the insoluble pellet was sonicated in 200 μL of 70% formic acid and subjected to ultracentrifugation at 300 000 *g* at 4°C for 30 min, and the soluble supernatant was collected.

Aβ levels

Brain $A\beta_{1-40}$ and $A\beta_{1-42}$ levels were measured using sandwich ELISA with a Human β Amyloid ELISA Kit (Wako Pure Chemical Industries, Ltd.) according to the manufacturer's instructions. BAN50 is a monoclonal antibody raised against a synthetic peptide of human $A\beta_{1-16}$; it preferentially reacts with the N-terminal portion of human Aβ starting at Asp-1 but does not cross-react with N-terminally truncated Aβ nor with rodent-type Aβ. BA27 and BC05, which specifically recognize the C terminus of $A\beta_{1-40}$ and $A\beta_{1-42}$, respectively, were conjugated with horseradish peroxidase and used as detector antibodies. Mice brain insoluble fractions described above were neutralized and subjected to BAN50/BA27 or BAN50/BC05 ELISA. The amount of Aβ was calculated by comparing these absorbance values with those of control solutions without herbal extract.

Aβ oligomerization analysis

Amount of $A\beta_{1-42}$ oligomer was measured using Aβ Aggregate Human Singleplex Bead Kit (Invitrogen Corporation, Carlsbad, CA, USA) according to the manufacturer's instructions. Data analysis was performed by a flow cytometer (FACSCaliber, Becton Dickinson Immunocytometry Systems, Franklin Lakes, NJ, USA).

Cell viability assay

SK-N-SH cells were maintained in Dulbecco's modified Eagle's medium (Gibco Life Technologies, Carlsbad, CA, USA) supplemented with 10% fetal calf serum and 4 mM L-glutamine in a humidified atmosphere of 5% CO_2 and 95% air. SK-N-SH cells were seeded in 96-well plates at a density of 1×10^4 cells per well. After 24 h, we pre-incubated SK-N-SH cells for 30 min with PGG, followed by 24 h treatment with 10 μM aggregated $A\beta_{1-42}$. Cell

viability was assessed using the 3-(4,5-dimethylthiazol-2-yl)-2,5-diphenyltetrazolium bromide (MTT) method. Absorbance values of formazan were determined at 590 nm with an automatic microplate reader.

Data analysis

Data were expressed as mean ± SD. Statistical comparisons were made using ANOVA with Bonferroni's *post hoc* analysis. $p < 0.05$ was considered to be significant.

Results

Concentration-dependent effects of *Paeonia suffruticosa* on kinetics of Aβ fibril formation and breakdown

In our previous publication, it was noted that several medicinal herbs including *Uncaria rhynchophylla*, *Cinnamomum cassia*, and *Paeonia suffruticosa* showed destabilizing activity on Aβ fibrils (Fujiwara *et al.* 2006). *Paeonia suffruticosa* which was extracted either by water, methanol, or ethanol was concentrated under reduced pressure to yield oily residues (2.33, 1.89, and 2.14 g for water, methanol, and ethanol, respectively). To examine the inhibitory effect of *Paeonia suffruticosa* on Aβ fibril formation, concentration-dependencies were examined by the thioflavin T method. We observed that fluorescence intensity in $A\beta_{1-40}$ and $A\beta_{1-42}$ declined in a concentration-dependent manner (Fig. 1a and b). $A\beta_{1-40}$ fibril formation was inhibited by 10 μg/mL of the water (48.5 ± 0.3%), methanol (40.1 ± 2.8%), and ethanol (34.6 ± 0.2%) extracts of *Paeonia suffruticosa*. $A\beta_{1-42}$ fibril formation was also inhibited by each of the three different extracts (10 μg/mL), although the inhibitory concentration was lower than for $A\beta_{1-40}$.

In the analysis of fibril destabilization, fluorescence derived from thioflavin T was decreased in a dose-dependent manner after the addition of each of the extracts of *Paeonia suffruticosa* to pre-formed Aβ fibrils, and the degree of inhibition was similar to that observed on Aβ aggregation (Fig. 1c and d). Pre-formed $A\beta_{1-40}$ fibrils were destabilized by 10 μg/mL of the water (58.2 ± 3.7%), methanol (74.9 ± 1.1%) and ethanol (71.7 ± 1.0%) extracts. Over 80% of pre-formed $A\beta_{1-40}$ and $A\beta_{1-42}$ fibrils were destabilized by each of the three different extracts at the concentration of 100 μg/mL.

Step-through passive-avoidance tests

Step-through passive-avoidance tests were carried out in Tg2576 mice at 11 to 14 months of age. In the first acquisition trial of the learning stage, all mice (11 months

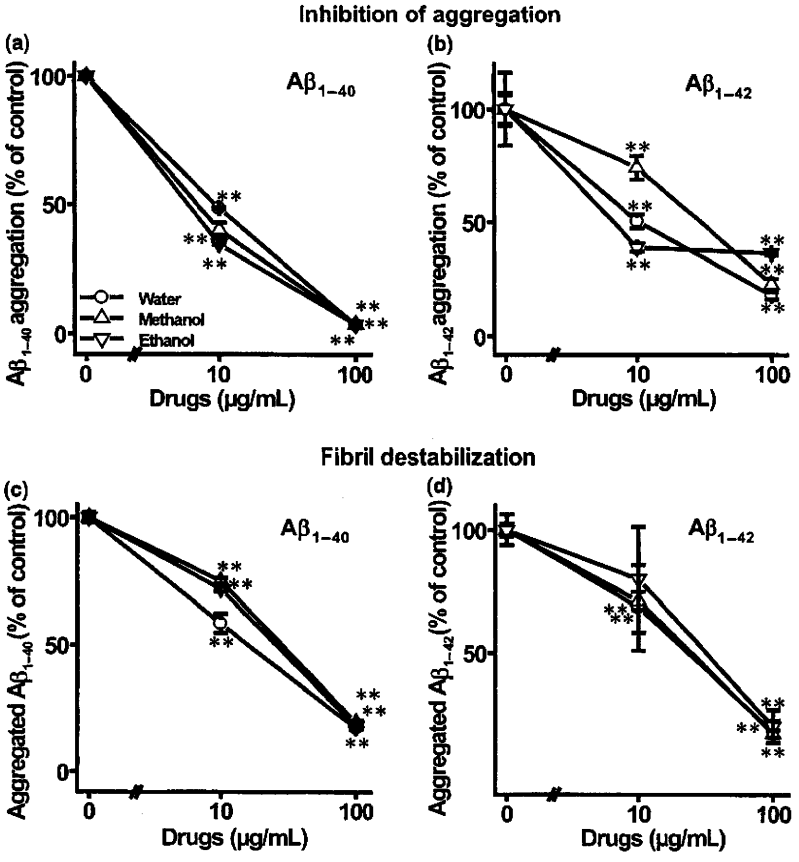

Fig. 1 Effects of three different *Paeonia suffruticosa* extracts on the kinetics of Aβ formation and destabilization. a and b: Aβ aggregate-formation assay. Reaction mixtures containing 20 μM of $A\beta_{1-40}$ (a) or $A\beta_{1-42}$, (b) 50 mM phosphate buffer (pH 7.4), and various extracts [water (circles), methanol (upward-pointing triangles), and ethanol (downward-pointing triangles)] were incubated at 37°C for 96 h (a) or 24 h (b). Aβ aggregation was expressed as percentage of the control sample which did not contain herbal extract. c and d: Aβ aggregate-destabilization assay. Reaction mixtures containing 20 μM $A\beta_{1-40}$ (c) or $A\beta_{1-42}$ (d) were incubated at 37°C for 96 h (c) or 24 h (d). The extracts were then added and incubated for another 30 min. Aβ aggregation was assessed by the thioflavin T method and expressed as the percentage of control aggregation in the absence of herbal extract. Values represent mean ± SD from four independent experiments. $^{**}p < 0.01$ compared with extract-untreated control.

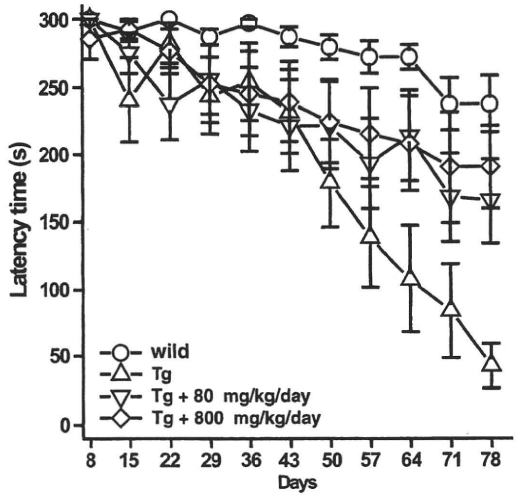

Fig. 2 Step-through latencies in the retention stages of the passive-avoidance task in *Paeonia suffruticosa*-treated transgenic (Tg2576) mice. Wild type and transgenic mice could acquire the avoidance memory by four or five repeated learning trials. The retention trials were carried out once per week for 10 weeks from Days 8 to 78 to evaluate the retention of avoidance memory. The latency time was measured for up to 300 s without delivering foot-shock. Wild type (Wild: circles); transgenic mice (Tg: upward-pointing triangles); 80 mg/kg/day *Paeonia suffruticosa* by repeated oral administration (Tg + 80 mg/kg/day: downward-pointing triangles), and 800 mg/kg/day *Paeonia suffruticosa* (Tg + 800 mg/kg/day: diamond). Values represent the means ± SD from 11 to 17 independent experiments.

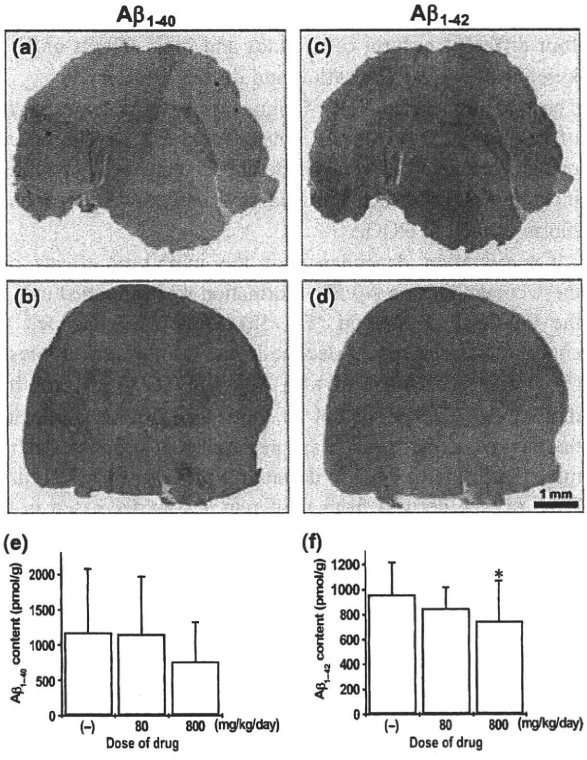

Fig. 3 Immunostaining (a–d) and ELISA analysis of formic acid-extractable Aβ levels (e and f) after dietary intake of *Paeonia suffruticosa* in Tg2576 mice. (a–d) Hemibrain cryostat sections were labeled with anti-$A\beta_{1-40}$ (a and b) and $A\beta_{1-42}$ (c and d) antibody. Image analysis was performed on the cerebral cortex from untreated (a and c) and *Paeonia suffruticosa*-treated (b and d) animals. Scale bar = 1 mm. Levels of $A\beta_{1-40}$ (e) and $A\beta_{1-42}$ (f) were quantified using an ELISA kit on formic acid-extractable Aβ from cortices of the low intake group (80 mg/kg/day) and high intake group (800 mg/kg/day). Values represent mean ± SD from 11 to 17 independent experiments. $^*p < 0.05$ compared with *Paeonia suffruticosa*-untreated control.

old) in the wild type and Tg groups entered the dark compartment immediately after being placed in the illuminated compartment. Repeating the acquisition trial increased the latency times in both groups. All mice in the wild type and Tg groups acquired avoidance memory, staying in the illuminated compartment for over 300 s on the fifth acquisition day. However, no significant differences were observed in the mean latency times between the wild type and Tg groups on any given day during the learning stage (data not shown). In retention trials (Fig. 2), the step-through latency of the Tg group was significantly reduced when compared with that of the wild type group. *Paeonia suffruticosa*-treated Tg mice were indistinguishable from non-transgenic littermates on days from 50 to 78 of testing.

Aβ pathology was reduced in *Paeonia suffruticosa*-treated Tg mice

To determine whether oral *Paeonia suffruticosa* treatment affected the accumulation of Aβ in brain tissue, we evaluated Aβ immunoreactivity in brain sections from untreated (Fig. 3a and c) and *Paeonia suffruticosa*-treated mice (Fig. 3b and d) using BA27 and BC05 antibodies which recognize the C-terminus of human $A\beta_{1-40}$ (Fig. 3a and b) and $A\beta_{1-42}$ (Fig. 3c and d). The number of Aβ-positive spots in the cortex and hippocampus were obviously lower in the *Paeonia suffruticosa*-treated mice compared with the untreated mice. No Aβ immunoreactivity was observed in brain sections from non-transgenic mice (data not shown).

We next measured the levels of $A\beta_{1-40}$ and $A\beta_{1-42}$ in brain tissue samples from Tg mice using a sensitive ELISA method (Fig. 3e and f). Consistent with the results of Aβ immunostaining, the $A\beta_{1-42}$ concentration in the samples from *Paeonia suffruticosa*-treated Tg mice (800 mg/kg/day) was significantly lower than the concentration in *Paeonia suffruticosa*-untreated mice (747.8 ± 322.4%, $p < 0.05$). In contrast to its effect on $A\beta_{1-42}$ levels, *Paeonia suffruticosa* treatment had no significant effect on $A\beta_{1-40}$ levels in the Tg mice. The levels of $A\beta_{1-40}$ and $A\beta_{1-42}$ were below the limit of detection in cerebral cortex samples from non-transgenic mice (data not shown).

HPLC analyses of *Paeonia suffruticosa*: identification of four different natural compounds and their effects on the kinetics of $A\beta_{1-42}$ formation and destabilization

The three-dimensional-HPLC fingerprints of water extracts of *Paeonia suffruticosa* are illustrated in Fig. 4. The water extract contained several different chemical compounds including paeonol, benzoic acid, and derivatives of paeoniflorin as well as PGG.

Concentration dependence of the inhibitory effects of these compounds on Aβ fibril formation was examined using the thioflavin T method (Fig. 5a). Only PGG induced a concentration-dependent decline in the thioflavin T fluorescence intensity associated with $A\beta_{1-42}$. PGG (3 μM) inhibited $A\beta_{1-42}$ fibril formation by more than 50%. Additional thioflavin-T experiments were performed in order to determine the ability of PGG to destabilize pre-formed Aβ fibrils. Fluorescence derived from thioflavin T was decreased in a dose-dependent manner after the addition of PGG to preformed Aβ fibrils to an extent similar to that seen for the inhibition of Aβ aggregation (Fig. 5b).

Next, we incubated different concentrations of PGG with unpolymerized $A\beta_{1-42}$ (10 μM) and monitored the formation of amyloid using the Thioflavin T method (Fig. 6). In the absence of PGG, $A\beta_{1-42}$ formed Thioflavin T-binding aggregates after a lag phase of 2 h, whereas thioflavin T signals were decreased to 33.6 ± 16.8% by 1 μM PGG after a lag phase of 24 h. Moreover, $A\beta_{1-42}$ aggregation was completely inhibited by 100 μM PGG.

Effect of PGG on $A\beta_{1-42}$ oligomers

To further characterize the breakdown products that accumulated in the presence of PGG, aliquots of $A\beta_{1-42}$ oligomerization reaction mixtures in the presence or absence of PGG were assayed by flow cytometric analysis (Fig. 7). In the absence of PGG, the fluorescence intensity of $A\beta_{1-42}$ oligomerized sample was potent compared with vehicle sample without $A\beta_{1-42}$ oligomers (Fig. 7a and b). Samples treated with PGG reduced the fluorescence intensity in a concentration-dependent manner (Fig. 7c–e). These data confirmed that PGG was a strong inhibitor of $A\beta_{1-42}$ oligomerization.

Neuroprotective effects of PGG against Aβ toxicity

To evaluate whether PGG could potentially prevent Aβ-induced toxicity, we pre-incubated SK-N-SH cells for 30 min with PGG, followed by 24 h treatment with 10 μM aggregated $A\beta_{1-42}$. SK-N-SH cell viability was significantly impaired by Aβ peptides, measured by MTT assay. PGG (10 μM) significantly protected SK-N-SH cells against Aβ-induced toxicity. When measured by MTT reduction, cell survival was restored from 56.9 ± 2.5% to 87.0 ± 13.6% in response to the $A\beta_{1-42}$ aggregates (Fig. 8).

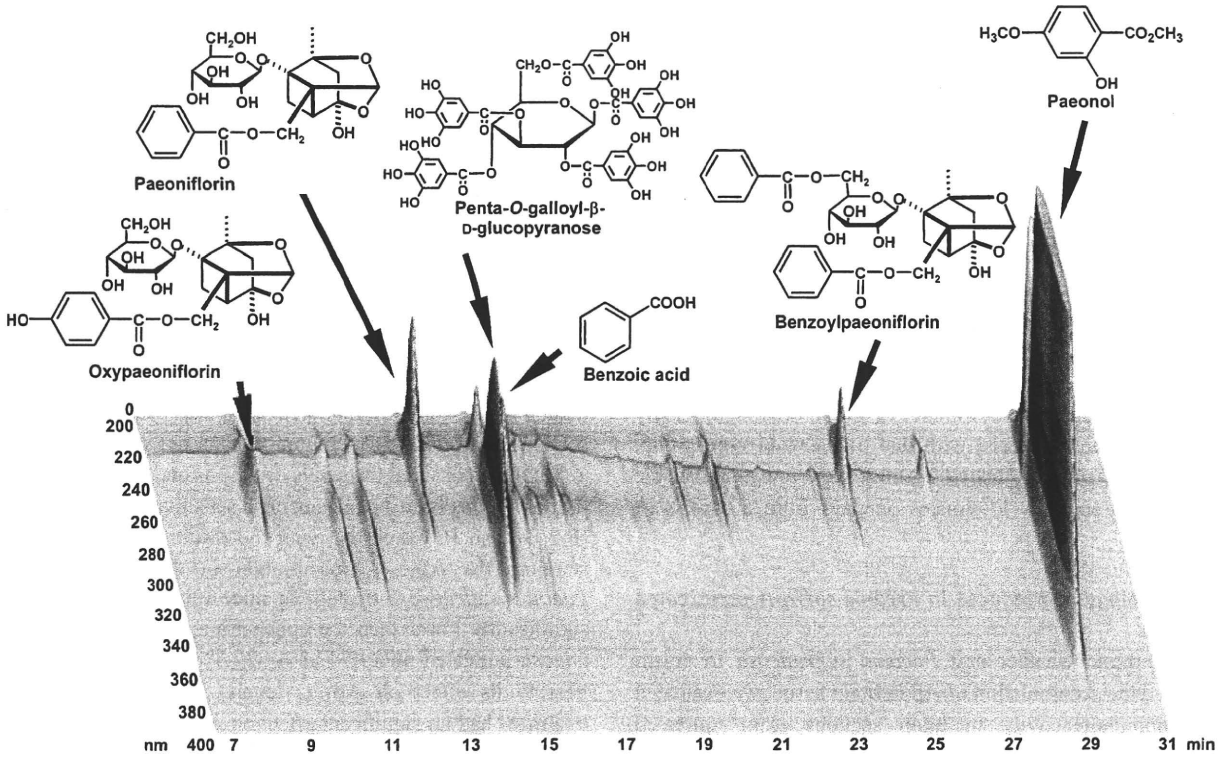

Fig. 4 Identification of chemicals by three-dimensional HPLC analysis of the water extract of *Paeonia suffruticosa*. Each peak indicates a molecule described in the figure.

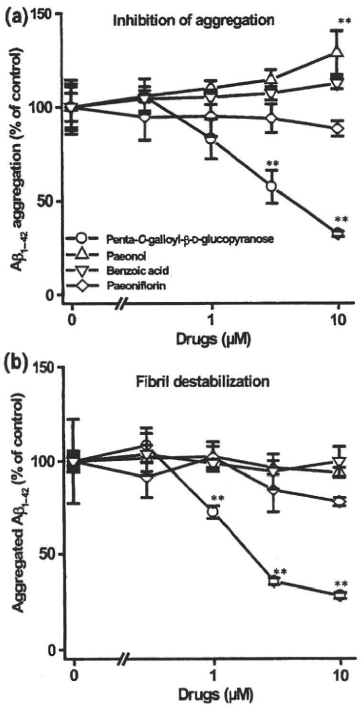

Fig. 5 Effects of distinct compounds isolated from *Paeonia suffruticosa* on the kinetics of Aβs formation and destabilization. a: Aβ aggregate-formation assay. Reaction mixtures containing 20 μM of $A\beta_{1-42}$, 50 mM phosphate buffer (pH 7.4), and various compounds [1,2,3,4,6-penta-*O*-galloyl-β-D-glucopyranose (circles), paeonol (upward-pointing triangles), benzoic acid (downward-pointing triangles), and paeoniflorin (diamond)] were incubated at 37°C for 24 h. Aβ aggregation is expressed as percentage of control observed in the absence of test compounds. b: Aβ aggregate-destabilization assay. Reaction mixtures containing 20 μM $A\beta_{1-42}$ were incubated at 37°C for 24 h. The extracts were added and incubated for 30 min. Aβ aggregation was assessed by the thioflavin T method and expressed as percentage of control aggregation observed in the absence of test compounds. Values represent mean ± SD from four independent experiments. $^{**}p < 0.01$ compared with extract-untreated control.

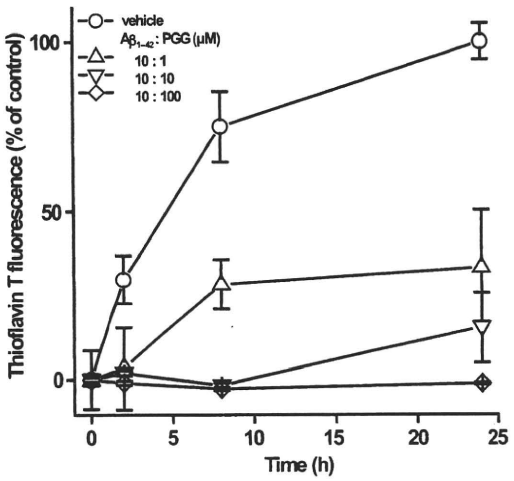

Fig. 6 The molar ratio of the Aβ–PGG interaction. Reaction mixtures containing 10 μM $A\beta_{1-42}$: PGG [solvent alone (circles), molar ratio 10 : 1 (upward-pointing triangles), 10 : 10 (downward-pointing triangles), and 10 : 100 (diamond)] were incubated at 37°C for indicated time. Thioflavin T fluorescence was expressed as a percentage of control which was observed at the point of 24 h without PGG. Values represent mean ± SD from four independent experiments.

Aβ pathology is diminished in PGG-treated Tg mice

To determine the effect of oral PGG treatment accumulation of Aβ in Tg type mice, we evaluated Aβ immunoreactivity in brain sections from untreated and PGG-treated mice by using antibodies BA27 and BC05 (Fig. 9a–d). The number of Aβ-positive spots in the hippocampus was obviously lower in PGG-treated mice (Fig. 9b and d) compared with untreated mice (Fig. 9a and c). No Aβ immunoreactivity was observed in brain sections from non-transgenic mice (data not shown).

We next measured the levels of $A\beta_{1-40}$ and $A\beta_{1-42}$ in brain samples from Tg mice by using a sensitive ELISA method (Fig. 9e and f). In the brains of Tg mice treated with PGG by repeated oral administration, the $A\beta_{1-40}$ and $A\beta_{1-42}$ concentrations were significantly lower (2417.5 ± 279.5% and 46.8 ± 3.0%, $p < 0.01$) than those in PGG-untreated mice. The levels of $A\beta_{1-40}$ and $A\beta_{1-42}$ were below the limit of detection in cerebral cortex samples from non-transgenic mice (data not shown).

Discussion

In AD research, much attention has focused on altering the course of the disease through early diagnosis and intervention. Clinical application of biomarkers and amyloid imaging may be attractive and realistic diagnostic procedures by which to identify the disease early. On the other hand, safety is an important concern with regard to early intervention with disease modifying drugs. *Paeonia suffruticosa* has been used medicinally in humans for more than 1000 years with virtually no toxic effects reported.

The results of our studies using thioflavin T fluorescence demonstrated that *Paeonia suffruticosa* extracts, regardless of the extraction method used, could inhibit the assembly of Aβ fibrils. All three extracts (water, methanol, and ethanol) induced a dramatic decline in the fluorescence intensity of thioflavin T in the μg/mL range. In our preliminary experiment, we confirmed that these extracts did not quench thioflavin T fluorescence at the indicated concentrations. These results suggest two possibilities; one is that *Paeonia suffruticosa* indeed destabilizes Aβ fibrils, and the other is that it antagonizes the binding of thioflavin T to Aβ. It has been reported that absorbance of Congo red was increased by binding to Aβ protein as well as to thioflavin T. The binding site in Aβ to Congo red was different from that to thioflavin

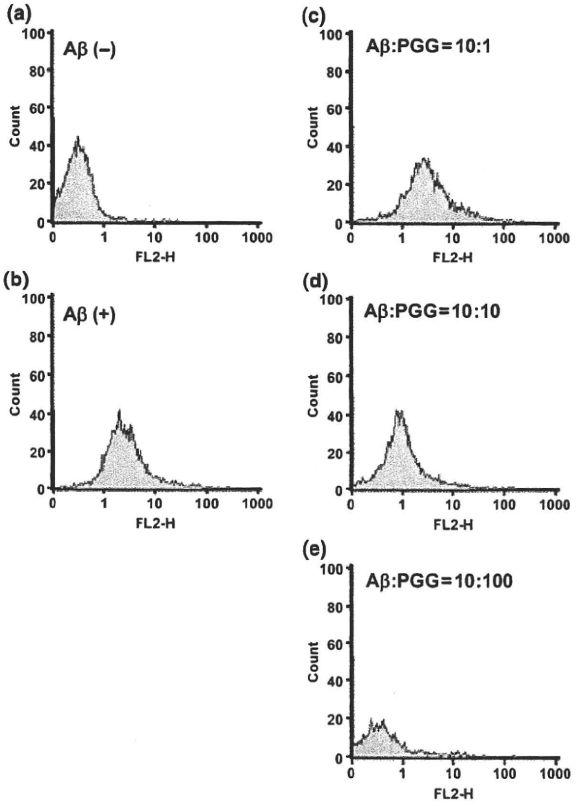

Fig. 7 Effects of PGG on $A\beta_{1-42}$ oligomeric species. These histograms were developed using reagents provided in the Aggregated Aβ Assay Kit. a: buffer-control; b: 10 μM $A\beta_{1-42}$ in absent of PGG; c–e: 10 μM $A\beta_{1-42}$ with PGG molar ratio 10 : 1 (c), 10 : 10 (d), and 10 : 100 (e).

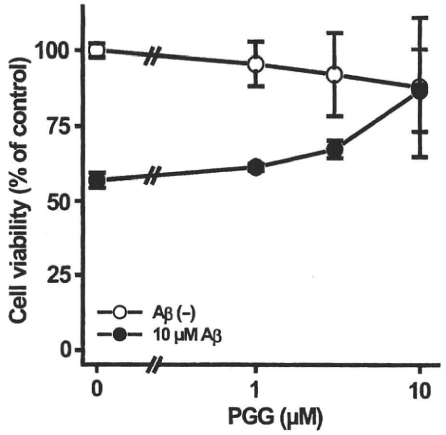

Fig. 8 Effects of PGG against Aβ-induced toxicity. SK-N-SH cells were pre-treated without or with PGG for 30 min followed by incubation without or with $A\beta_{1-42}$ (10 μM) for 24 h. Cell viability was assessed by MTT method and expressed as a percentage of control viability, which was observed in the absence of $A\beta_{1-42}$ and PGG. Values represent the means ± SD from four independent experiments.

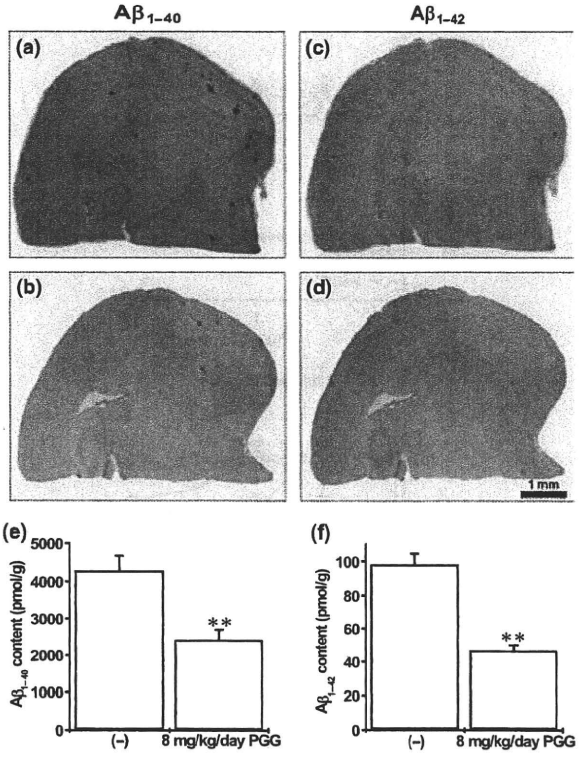

Fig. 9 Immunostaining (a–d) and ELISA analysis of formic acid-extractable Aβ levels (e and f) after dietary intake of 1,2,3,4,6-penta-*O*-galloyl-β-D-glucopyranose (PGG) in Tg2576 mice. (a–d) Hemibrain cryostat sections were labeled with anti- $A\beta_{1-40}$ (a and b) and $A\beta_{1-42}$ (c and d) antibody. Image analysis was performed on the cerebral cortices from PGG-untreated (a and c) and -treated (b and d) animals. Scale bar = 1 mm. Levels of $A\beta_{1-40}$ (e) and $A\beta_{1-42}$ (f) were quantified on formic acid-extractable Aβ from cortices of the 8 mg/kg/day PGG groups. Values represent mean ± SD from seven to eight independent experiments. $^{**}p < 0.01$, compared with PGG-untreated control.

T. In our experiments, each of the three *Paeonia suffruticosa* extracts decreased the absorbance of Congo red (data not shown), suggesting that the decrease in thioflavin T fluorescence by *Paeonia suffruticosa* extracts was caused by destabilization of Aβ fibrils. Moreover, our preliminary atomic force microscopy data also strongly support this notion, as destabilization of Aβ fibrils by *Paeonia suffruticosa* extracts was directly visualized (data not shown). The extracts of *Paeonia suffruticosa* inhibited aggregation of both $A\beta_{1-40}$ and $A\beta_{1-42}$ to a similar extent. Therefore, the inhibitory effect of *Paeonia suffruticosa* on amyloidogenesis of Aβ may not be dependent on the distinct amino acid sequence of its C-terminal.

Paeonia suffruticosa treatment prevented Aβ-related memory deficits and AD-type neuropathology *in vivo*. In our study, we found that treatment of Tg2576 mice with *Paeonia suffruticosa* attenuated memory deterioration, and this effect coincided with an approximately 20% reduction in

Aβ peptide content in the brain. We hypothesize that treatment with *Paeonia suffruticosa* may have beneficial effects on AD-type memory deterioration through a direct interaction between *Paeonia suffruticosa* and Aβ peptides in the brain, leading to the prevention of Aβ plaque formation.

Our studies also showed that PGG at low concentrations (IC_{50} = 3 μM) can inhibit Aβ aggregation or promote its destabilization. Moreover, our preliminary scanning electron microscopy data also strongly support this notion, as destabilization of Aβ fibrils by PGG was directly visualized (Fig. S1). As other chemical compounds, such as paeonol, benzoic acid, and paeoniflorin had no effects on Aβ aggregation, PGG may be the principal active constituent responsible for the effect of *Paeonia suffruticosa* on Aβ fibril regulation. Previous published literatures reported that several polyphenols, such as those from green tea or grape, had anti-aggregation property (Ehrnhoefer *et al.* 2008; Rivière *et al.* 2008). PGG had a comparable inhibitory effect with such published polyphenols.

The toxicity of Aβ is becoming more strongly linked to the formation of oligomeric aggregates (Kirkitadze *et al.* 2002). In our experiments, PGG inhibited Aβ oligomerization. Moreover, treatment of SK-N-SH cells with PGG significantly protected the cells from $Aβ_{1–42}$ toxicity at concentrations similar to those that inhibited Aβ aggregation. Thus, our experiments suggest that PGG inhibited not only Aβ fibril formation but also neurotoxic Aβ oligomer formation. Furthermore, oral intake of PGG reduced Aβ plaque burden and Aβ peptide content in brain tissue from Tg2576 mice, as did like *Paeonia suffruticosa*. There are two possible explanations; one is that PGG indeed destabilizes Aβ fibrils, and the other is that it inhibits the Aβ production or its secretion in Tg2576 mice brain. We demonstrated that PGG did not affect the level of full-length APP in Tg2576 mice (Figure S2), suggesting that the decrease in Aβ plaques and Aβ peptide content in brain tissue from Tg2576 mice by PGG may be caused by destabilization of Aβ fibrils. Curcumin, an active compound of *Curcuma longa*, was reported to inhibit Aβ fibril formation and to destabilize preformed Aβ fibrils *in vitro* and *in vivo* (Ono *et al.* 2004; Yang *et al.* 2005). It has also been reported that this compound is highly hydrophobic and should readily enter the brain to bind to plaques *in vivo* (Yang *et al.* 2005). Although highly hydrophilic, unlike curcumin, PGG has curcumin-like activity on Aβ fibril regulation *in vivo*. Studies of the metabolism of PGG and its ability to penetrate the blood-brain barrier by this compound are now underway.

In conclusion, our study demonstrates that *Paeonia suffruticosa* and PGG not only inhibit Aβ fibril formation but also disassemble pre-formed Aβ fibrils. Moreover, our experiments suggest that PGG inhibits Aβ oligomerization and Aβ toxicity. As a result, it improved memory deficits in Tg2576 mice. Therefore, extracts of *Paeonia suffruticosa* and PGG could have potential as therapeutic drugs for AD patients and may also be useful as primary or secondary preventive agents for healthy individuals and patients with mild cognitive impairment. Furthermore, *Paeonia suffruticosa* has a satisfactory safety profile because no obvious adverse effects of *Pilulae octo-medicamentorum rehmanniae* have been reported. In our preliminary experiments, *Paeonia suffruticosa* was tested for hepatotoxicity, nephrotoxicity, and other biochemical parameters in transgenic mice. Fortunately, this medicinal herb did not show any signs of organ toxicity. Thus, *Paeonia suffruticosa* appears to be a safe natural product for regulating Aβ aggregation. *Paeonia suffruticosa* and PGG may represent a new class of therapeutic and preventive agents for AD which act to regulate the formation and the clearance of senile plaques.

Acknowledgements

This work was partially supported by (i) a grant-in-aid for scientific research from the Ministry of Education, Science, Sports and Culture of Japan (#16590554), (ii) a program for the promotion of fundamental studies in Health Science of the National Institute of Biomedical Innovation (NIBIO) of Japan (#03-1), and (iii) a grant-in-aid from Core Research for Evolutional Science and Technology of Japan Science and Technology Corporation. We thank S. Isogami and M. Takahashi for kind advice and technical supports.

Supporting Information

Additional Supporting Information may be found in the online version of this article:

Figure S1 Scanning electron microscope imaging of $Aβ_{1-42}$ fibrils. After incubation of $Aβ_{1-42}$ for 24 h for preformed fibrils, the mixture of aggregated Aβ and the PGG was incubated at 37°C for 1 h. A: vehicle (DMSO); B: 10 μM $Aβ_{1-42}$: 10 μM PGG (molar ratio 1 : 1). Scale bar = 5 μm.

Figure S2 Effects of PGG on the level of amyloid precursor protein (APP) in Tg2576 mice. Immunoblotting of brain levels of APP after dietary 1,2,3,4,6-penta-*O*-galloyl-β-D-glucopyranose (PGG) in Tg2576. Levels of APP were quantitated by immunoblotting with full length APP antibody from cortices of 8 mg/kg/day-PGG groups. The samples were separated on a 10% polyacrylamide gel, followed by immunoblotting with anti-full length APP antibody. Arrowheads point to APP. Similar results were obtained from at least 3 independent experiments.

Please note: Wiley-Blackwell are not responsible for the content or functionality of any supporting materials supplied by the authors. Any queries (other than missing material) should be directed to the corresponding author for the article.

References

Anderton B. H., Callahan L., Coleman P. *et al.* (1998) Dendritic changes in Alzheimer's disease and factors that may underlie these changes. *Prog. Neurobiol.* **55**, 595–609.

Barghorn S., Nimmrich V., Striebinger A. *et al.* (2005) Globular amyloid beta-peptide oligomer – a homogenous and stable neuropathological protein in Alzheimer's disease. *J. Neurochem.* **95**, 834–847.

Barrow C. J. and Zagorski M. G. (1991) Solution Structures of β-peptide and its constituent fragments: relation to amyloid deposition. *Science* **253**, 179–182.

Calon F., Lim G. P., Yang F. *et al.* (2004) Docosahexaenoic acid protects from dendritic pathology in an Alzheimer's disease mouse model. *Neuron* **43**, 633–645.

Chou T. C. (2003) Anti-inflammatory and analgesic effects of Paeonol in carrageenan-evoked thermal hyperalgesia. *Br. J. Pharmacol.* **139**, 1146–1152.

Darreh-Shori T., Hellstrom-Lindahl E., Flores-Flores C. *et al.* (2004) Long-lasting acetylcholinesterase splice variations in anticholinesterase-treated Alzheimer's disease patients. *J. Neurochem.* **88**, 1102–1113.

Ehrnhoefer D. E., Bieschke J., Boeddrich A. *et al.* (2008) EGCG redirects amyloidogenic polypeptides into unstructured, off-pathway oligomers. *Nat. Struct. Mol. Biol.* **15**, 558–566.

Fujiwara H., Iwasaki K., Furukawa K. *et al.* (2006) *Uncaria rhynchophylla*, a Chinese medicinal herb, has potent antiaggregation effects on Alzheimer's beta-amyloid proteins. *J. Neurosci. Res.* **84**, 427–433.

Hofmann T., Glabasnia A., Schwarz B. *et al.* (2006) Protein binding and astringent taste of a polymeric procyanidin, 1,2,3,4,6-penta-*O*-galloyl-beta-D-glucopyranose, castalagin, and grandinin. *J. Agric. Food. Chem.* **54**, 9503–9509.

Hsieh C. L., Cheng C. Y. and Tsai T. H. (2006) Paeonol reduced cerebral infarction involving the superoxide anion and microglia activation in ischemia-reperfusion injured rats. *J. Ethnopharmacol.* **106**, 208–215.

Iwasaki K., Kobayashi S., Chimura Y. *et al.* (2004) A randomized, double-blind, placebo-controlled clinical trial of the Chinese medicinal herb "ba wei di huang wan" in the treatment of dementia. *J. Am. Geriatr. Soc.* **52**, 1518–1521.

Iwasaki K., Satoh-Nakagawa T., Maruyama M. *et al.* (2005) A randomized, observer-blind, controlled trial of the traditional Chinese medicine Yi-Gan San for improvement of behavioral and psychological symptoms and activities of daily living in dementia patients. *J. Clin. Psychiatry* **66**, 248–252.

Kirkitadze M. D., Bitan G. and Teplow D. B. (2002) Paradigm shifts in Alzheimer's disease and other neurodegenerative disorders: the emerging role of oligomeric assemblies. *J. Neurosci. Res.* **69**, 567–577.

Le Bars P. L., Katz M. M., Berman N. *et al.* (1997) A placebo-controlled, double-blind, randomized trial of an extract of Ginkgo biloba for dementia. North American EGb Study Group. *JAMA* **278**, 1327–1332.

Li Y., Kim J., Li J. *et al.* (2005) Natural anti-diabetic compound 1,2,3,4,6-penta-*O*-galloyl-D-glucopyranose binds to insulin receptor and activates insulin-mediated glucose transport signaling pathway. *Biochem. Biophys. Res. Commun.* **336**, 430–437.

Lin H. C., Ding H. Y., Ko F. N. *et al.* (1999) Aggregation inhibitory activity of minor acetophenones from *Paeonia* species. *Planta Med.* **65**, 595–599.

Millard C. B. and Broomfield C. A. (1995) Anticholinesterases: medical applications of neurochemical principles. *J. Neurochem.* **64**, 1909–1918.

Nakagawasai O., Yamadera F., Iwasaki K. *et al.* (2004) Effect of kami-untan-to on the impairment of learning and memory induced by thiamine-deficient feeding in mice. *Neuroscience* **125**, 233–241.

Ono K., Hasegawa K., Naiki H. *et al.* (2004) Curcumin has potent anti-amyloidogenic effects for Alzheimer's beta-amyloid fibrils in vitro. *J. Neurosci. Res.* **75**, 742–750.

Park C. H., Lee Y. J., Lee S. H. *et al.* (2000) Dehydroevodiamine HCl prevents impairment of learning and memory and neuronal loss in rat models of cognitive disturbance. *J. Neurochem.* **74**, 244–253.

Rivière C., Richard T., Vitrac X. *et al.* (2008) New polyphenols active on beta-amyloid aggregation. *Bioorg. Med. Chem. Lett.* **18**, 828–831.

Selkoe D. J. (2002) Alzheimer's disease is a synaptic failure. *Science* **298**, 789–791.

Suemoto T., Okamura N., Shiomitsu T. *et al.* (2004) *In vivo* labeling of amyloid with BF-108. *Neurosci. Res.* **48**, 65–74.

Suzuki T., Arai H., Iwasaki K. *et al.* (2001) A Japanese herbal medicine (Kami-Untan-To) in the treatment of Alzheimer's disease: A pilot study. *Alzheimer's Rep.* **4**, 177–182.

Tierney M. C., Fisher R. H., Lewis A. J. *et al.* (1988) The NINCDS-ADRDA Work Group criteria for the clinical diagnosis of probable Alzheimer's disease: a clinicopathologic study of 57 cases. *Neurology* **38**, 346–359.

Wirths O., Multhaup G. and Bayer T. A. (2004) A modified β-amyloid hypothesis: intraneuronal accumulation of the β-amyloid peptide – the first step of a fatal cascade. *J. Neurochem.* **91**, 513–520.

Yang F., Lim G. P., Begum A. N. *et al.* (2005) Curcumin inhibits formation of amyloid beta oligomers and fibrils, binds plaques, and reduces amyloid in vivo. *J. Biol. Chem.* **280**, 5892–5901.

Yasuda T., Kon R., Nakazawa T. *et al.* (1999) Metabolism of Paeonol in rats. *J. Nat. Prod.* **62**, 1142–1144.

Journal of the Neurological Sciences 285 (2009) 100–108

Contents lists available at ScienceDirect

Journal of the Neurological Sciences

journal homepage: www.elsevier.com/locate/jns

Comparison study of amyloid PET and voxel-based morphometry analysis in mild cognitive impairment and Alzheimer's disease

Masaaki Waragai [a], Nobuyuki Okamura [b,*], Katsutoshi Furukawa [a], Manabu Tashiro [c], Shozo Furumoto [b,d], Yoshihito Funaki [e], Motohisa Kato [b], Ren Iwata [e], Kazuhiko Yanai [b], Yukitsuka Kudo [f], Hiroyuki Arai [a]

[a] Department of Geriatrics and Gerontology, Division of Brain Sciences, Institute of Development, Aging and Cancer, Tohoku University, Sendai, Japan
[b] Department of Pharmacology, Tohoku University School of Medicine, Sendai, Japan
[c] Division of Cyclotron Nuclear Medicine, Cyclotron and Radioisotope Center, Tohoku University, Sendai, Japan
[d] Department of Nuclear Medicine and Radiology, Institute of Development, Aging and Cancer, Tohoku University, Sendai, Japan
[e] Division of Radiopharmaceutical Chemistry, Cyclotron and Radioisotope Center, Tohoku University, Sendai, Japan
[f] Innovation of New Biomedical Engineering Center, Tohoku University, Sendai, Japan

ARTICLE INFO

Article history:
Received 27 February 2009
Received in revised form 5 May 2009
Accepted 2 June 2009
Available online 23 June 2009

Keywords:
Alzheimer's disease
Amyloid
Early diagnosis
Magnetic resonance imaging
Positron emission tomography
BF-227

ABSTRACT

Two techniques employed for the early diagnosis of dementia are the imaging of amyloid-β protein using positron emission tomography (PET) and voxel-based morphometry analysis of MRI (VBM-MRI). The purpose of this study was to evaluate the clinical utility of amyloid PET and VBM-MRI for the early diagnosis and tracking of the severity of Alzheimer's disease (AD). The neuritic plaque burden and gray matter losses were evaluated using [^{11}C]BF-227-PET and VBM-MRI in 12 healthy controls, 13 subjects with mild cognitive impairment (MCI), including 6 who converted to AD and 7 who did not convert, and 15 AD patients. The AD patients and the MCI converters exhibited a neocortical retention of BF-227 and parahippocampal gray matter loss shown by VBM-MRI. The MCI converters were more clearly distinguished from the MCI non-converters in BF-227-PET than VBM-MRI. The combined sample of the MCI converters and AD patients showed a significant correlation of MMSE scores with the global gray matter loss, but not with the BF-227 retention. These findings suggest that amyloid PET using [^{11}C]BF-227 is better suited for the prediction of conversion from MCI to AD, while VBM-MRI appears to be better suited for tracking the severity of dementia.

1. Introduction

Alzheimer's disease (AD) is a neurodegenerative disorder characterized by a progressive impairment of cognitive function and behavior. AD is the most common form of dementia, particularly in the elderly [1,2]. The pathological hallmarks of AD are extracellular amyloid-β protein deposits called senile plaques (SPs) and intracellular neurofibrillary tangles (NFTs), which occur together with selective neuronal and synaptic loss [3,4]. These changes are also associated with progressive neuronal loss and resultant cerebral atrophy [5]. The presence of both SPs and NFTs are prerequisites for a definitive diagnosis of AD, but more attention has been focused on the role of amyloid-β protein (Aβ) in the pathogenesis of AD. Although the mechanisms of development of AD have not been completely elucidated, Aβ is assumed to play a causal role in the pathology of AD.

In vivo imaging techniques that can non-invasively and reliably assess Aβ deposition are currently receiving considerable attention in the search for a method for early diagnosis of AD [6–11]. Pittsburgh Compound-B (PIB) is at present the most commonly used probe for Aβ and has been applied to the diagnosis of AD and several other neurological disorders [12–16]. For example, amnesic mild cognitive impairment (MCI) is currently considered a prodromal state of AD, though not all individuals with MCI will develop AD; MCI converters and non-converters are difficult to distinguish from a clinical and neuropsychological perspective. Analysis of PIB-PET images in MCI subjects revealed a bimodal distribution of PIB uptake in the neocortex. About two thirds of MCI cases showed neocortical retention of PIB similar in distribution (and sometimes in degree) to AD, while the other third of MCI cases showed no cortical retention, similar to normal individuals [15,17,18]. A previous PIB-PET study demonstrated higher PIB retention in MCI converters than in non-converters, suggesting the utility of amyloid imaging in the prediction of progression to dementia [18].

We have developed novel benzoxazole derivatives for in vivo imaging of amyloid [19–21]. One of these agents, 2-(2-[2-demethylaminothiazol-5-yl]ethenyl)-6-(2-[Fluoro]ethoxy)benzoxazole (BF-227), displayed a high binding affinity to Aβ fibrils, excellent brain uptake and specifically labels amyloid deposits in transgenic mice [20,22]. A clinical PET study using [^{11}C]BF-227 demonstrated higher retention of this tracer in the

* Corresponding author. Department of Pharmacology, Tohoku University School of Medicine, Tohoku University, 2-1 Seiryo-machi, Aoba-ku, Sendai 980-8575, Japan. Tel.: +81 22 717 8058; fax: +81 22 717 8060.
E-mail address: oka@mail.tains.tohoku.ac.jp (N. Okamura).

0022-510X/$ – see front matter
doi:10.1016/j.jns.2009.06.005

neocortex of AD patients than normal individuals [22]. There are several drawbacks to the use of this tracer, including its relatively low affinity to AD brain tissue ($K_d = 25$ nM) compared to PIB [23] and its slower clearance from the white matter region due to its higher lipophilicity (Log$P = 1.75$),[22] resulting in lower signal to background ratio than PIB–PET. However, the voxel-based analysis of BF-227–PET images indicated a pattern of tracer distribution distinct from that of PIB–PET.[12] Intriguingly, the preferential [^{11}C]BF-227 retention in the posterior neocortical region of the AD brain corresponded with an area containing a high density of neuritic plaques [4,22]. A preliminary report of the direct comparison of PIB–PET and BF-227–PET in the same AD patients additionally demonstrated a difference in the regional distribution of these two agents, which presumably reflects their different preference for various conformations of Aβ in the senile plaque generation process [24]. From these findings, we speculate that BF-227 detects neuritic plaques containing dense amyloid fibrils preferentially, compared to PIB–PET, and provides unique information about the Aβ pathology in AD patients. The early detection of Aβ deposition is important to begin medication to prevent a cognitive decline in the stage of MCI, since it appears that the deposition of Aβ starts earlier than the clinical diagnosis of dementia [25–27]. Approximately 20–30% of healthy, age-matched subjects exhibited neocortical retention of PIB, predominantly in the prefrontal and posterior cingulate cortices [15,16]. The demonstration of PIB retention in a proportion of normal individuals supports postmortem observations that Aβ aggregation predominantly occurs before the onset of dementia. However, there is currently no evidence that all PIB-positive normal individuals are destined to develop dementia. Highly sensitive detection of Aβ leads to a potential risk for misjudging the process of normal physiological aging as a pathological indicator of AD. The accurate prediction of AD progression is thus necessary to prevent the administration of non-essential treatments to individuals who are not at risk of converting to AD. In particular, a shift of brain Aβ from the soluble to fibrillar form is closely associated with onset of AD [28]. Thus, selective detection of dense amyloid fibrils would be advantageous to differentiate normal aging process from AD with high specificity, as the deposition of neuritic plaques is strongly associated with the earliest symptoms of AD [25]. Based on this background evidence, we anticipated that BF-227–PET would more accurately predict the conversion from MCI to AD than other imaging techniques.

Cognitive decline is reported to strongly correlate with cortical atrophy in AD, suggesting that cortical degeneration is the primary basis of cognitive decline in AD [5]. Thus, an increased rate of cerebral atrophy, as evaluated using MRI, is a diagnostic feature of AD that correlates with the clinical stage/severity and is thought to represent the macroscopic consequences of neuronal destruction [29–31]. Medial temporal lobe atrophy, as seen in MRI scans of AD patients, is a sensitive marker of AD even in its earliest stages. Volumetric analysis of the entorhinal cortex distinguished subjects who were destined to develop dementia from normal controls with high accuracy [32]. However, this approach is time-consuming and highly dependent on analyst expertise because it requires accurate manual outlining of the region of interest for the measurement. Voxel-based morphometry (VBM) has emerged as an ideal tool to visualize the changes in gray matter density in disease states. This technique has been reported to detect gray matter loss in MCI and AD patients. In addition, lower gray matter density has been reported in MCI converters compared with MCI non-converters [33–37]. These findings suggest that measurement of gray matter loss in the medial temporal lobe or the other regions might predict progression from MCI to AD with high accuracy. A direct comparison of MRI with PIB–PET was previously performed in the control, MCI and AD populations [38]. The distributions of hippocampal volume did not overlap between AD and normal control groups with the exception of one control subject, and MCI subjects are evenly distributed between the AD and normal controls. In contrast, PIB–PET uptake showed a bimodal distribution. While all AD subjects are tightly clustered in the high PIB retention range, both the normal control and MCI subjects segregate themselves into high and low PIB retention groups. The voxel-by-voxel comparisons of AD versus control patients revealed differences in the topographical distribution of amyloid deposition and in grey matter loss, suggesting that these two imaging strategies provide complementary information about AD pathology.

In this study, we performed amyloid-imaging PET using [^{11}C]BF-227 and VBM analysis of MRI images in subjects with MCI and AD. We investigated whether changes in BF-227 uptake and gray matter density were associated with later conversion to AD in MCI populations. Moreover, we examined the association of these measurements with cognitive function in AD and MCI converters to investigate whether these imaging strategies can track the severity of AD pathology.

2. Materials and methods

2.1. Staining of senile plaques using BF-227

Postmortem brain tissue from a 69-year-old male with autopsy-confirmed AD was obtained from Fukushimura Hospital (Toyohashi, Japan). Experiments were performed under the regulations of the hospital ethics committee. Serial sections (6 μm) taken from paraffin-embedded blocks of the temporal cortex were prepared in xylene and ethanol. Before BF-227 staining, quenching of autofluorescence was performed. The quenched tissue section was immersed in 100 μM of BF-227 containing 50% ethanol for 10 min. The section stained with BF-227 was then dipped briefly into water and rinsed in PBS for 60 min before coverslipping with FluorSave Reagent (Calbiochem, La Jolla, CA), and examined using an Eclipse E800 microscope (Nikon, Tokyo, Japan) equipped with a V-2A filter set (excitation 380–420 nm, dichroic mirror 430 nm, long pass filter 450 nm). An adjacent section was immunostained using a monoclonal antibody (mAb) against Aβ (6F/3D; Dako A/S, Glostrup, Denmark). After pretreatment with 90% formic acid for 5 min, sections were immersed in blocking solution for 30 min and then incubated for 60 min at 37 °C with 6F/3D at a dilution of 1:50. After incubation, sections were processed with the avidin–biotin method using a Pathostain ABC-POD(M) Kit (Wako, Osaka, Japan) and diaminobenzidine tetrahydrochloride.

2.2. Subjects

Patients recruited in the present study included 12 normal age-matched controls, 13 subjects with amnestic MCI, and 15 patients with AD. Diagnoses of probable AD were based on criteria from the National Institute of Neurological and Communicative Disorders and Stroke and the Alzheimer's Disease Related Disorders Association (NINCDS-ADRDA) [39]. The diagnosis of amnestic MCI was made according to the published criteria described previously [40]. All MCI subjects underwent medical and neuropsychological reevaluation at approximately 3 month intervals. Conversion to AD was diagnosed when (1) signs of deterioration of the general cognitive function were present and continued for at least 6 months, and (2) the patient's score on the Clinical Dementia Rating changed by more than 0.5 points. The MCI subjects were divided into two groups, MCI converters ($n = 6$) and MCI non-converters ($n = 7$). The MCI converters were defined as patients who eventually developed AD within a mean follow-up of 27.0 ± 7.9 months (range 14–30 months). The MCI non-converters were defined as having a transient memory loss or remaining cognitively stable through at least a 2 year follow-up (27.7 ± 2.2 months; range 25–30 months). The control group was recruited from volunteers who were not taking centrally-acting medications, had no cognitive impairment and had no cerebrovascular lesions identified via MRI. All subjects were screened using a questionnaire and medical history, and subjects with medical conditions potentially affecting the central nervous system were excluded. In addition, none

Table 1
Demographic characteristics of the subjects.

	Control	MCI non-converter	MCI converter	AD
N	12	7	6	15
Age (year)	67.3 ± 2.7	77.6 ± 3.1	80.2 ± 4.1	71.0 ± 5.1
Gender (F/M)	6/6	2/5	4/2	8/7
MMSE	29.9 ± 0.3	26.3 ± 1.1	25.7 ± 2.0	19.8 ± 3.5

of the subjects had asymptomatic cerebral infarction detected via T2-weighted MRI. Demographic data for the subjects are shown in Table 1. Although the MCI converters and non-converters were statistically older than the control subjects and the AD patients, no statistical difference in age was observed between the MCI converters and the non-converters. The AD patients showed a significantly lower MMSE score than the MCI converters, non-converters, and control subjects ($p<0.05$), however, no statistical difference in MMSE score was observed between the MCI converters and the non-converters. The Committee on Clinical Investigation at Tohoku University School of Medicine and the Advisory Committee on Radioactive Substances at Tohoku University approved the study protocol.

3. MRI methods

All subjects underwent MRI with a 1.5 T MR scanner (GE Signa Hispeed, Milwaukee, WI). A three-dimensional volumetric acquisition of a T1-weighted gradient echo sequence produced a gapless series of thin axial sections using a vascular TOF SPGR sequence (echo time/repetition time, 2.4/50 ms; flip angle, 45°; acquisition matrix, 256×256; 1 excitation; field of view, 22 cm; slice thickness, 2.0 mm). Cerebral atrophy was evaluated by VBM [41]. For spatial normalization, a 12-parameter affine transformation was used to avoid segmentation errors caused by the partial-volume effects inherently created by warping. The normalized MRI was then segmented into gray matter, white matter, cerebrospinal fluid, and other components using SPM2 or SPM5 software. The segmentation procedure involved calculating the Bayesian probability of each voxel belonging to each tissue class based on a priori MRI information with a non-uniformity correction. The segmented gray matter images were then subjected to affine and non-linear spatial normalization using a template of a priori gray matter. The spatially normalized gray matter images were smoothed with an isotropic Gaussian kernel (12 mm at full width at half maximum) using the partial-volume effects to create a spectrum of gray matter intensities. The resulting gray matter intensities were equivalent to the weighted average of gray matter voxels located in the volume fixed by the smoothing kernel. Regional intensities can thus be considered equivalent to gray matter concentration. Differences of gray matter intensities between groups were assessed using a *t*-test with a height threshold of $p<0.05$, corrected for multiple comparisons by the family-wise error method. The extent threshold was set to 100 voxels. Parahippocampal gray matter density was additionally evaluated by calculating the average intensities in the bilateral parahippocampal region of interest (ROI) using Dr.View/LINUX software (AJS, Japan). To evaluate global atrophy, a *Z*-score map was created via the comparison of individual gray matter images with the mean and S.D. of gray matter images of healthy controls after voxel normalization to global mean intensities. The degree of global atrophy (% global atrophy) was calculated as a ratio of the area in which the *Z*-score of the voxel was more than 2.0 to whole brain area, using Voxel-Based Specific Regional Analysis System for AD (VSRAD) software (Eisai, Tokyo, Japan) [42].

3.1. PET procedure

Radiosynthesis of [^{11}C]BF-227 and the procedure used for BF-227–PET were performed as described previously. [22] BF-227 and its N-desmethylated derivative (a precursor of [^{11}C]BF-227) were custom-synthesized by Tanabe R&D Service Co. [^{11}C]BF-227 was synthesized from its precursor by N-methylation in dimethyl sulfoxide using [^{11}C]methyl triflate. The [^{11}C]BF-227–PET study was performed using a PET SET-2400W scanner (Shimadzu Inc., Japan). After an intravenous injection of 211–366 mBq [^{11}C]BF-227, dynamic PET images were obtained for 60 min with the subject's eyes closed. Standardized uptake value (SUV) images of [^{11}C]BF-227 were obtained by normalizing the tissue radioactivity concentration to the injected dose and body weight. ROIs were placed on individual axial MR images in the cerebellar hemisphere and the frontal, lateral temporal, parietal and posterior cingulate cortices. The ROI information was then copied onto the dynamic PET SUV images, and regional SUVs were sampled using Dr.View/LINUX software. The ratio of the regional to cerebellar SUV (SUVR) at 40–60 min post-injection was calculated, and averaged SUVR values in the frontal, temporal, parietal and posterior cingulate cortices were considered representative of BF-227 retention in the neocortex (neocortical SUVR).

3.2. Statistical analysis

Statistical comparison of PET and MRI measurements in the four groups was performed via an analysis of variance followed by a Bonferroni multiple comparisons test with a significance level of $p<0.05$. Statistical comparisons of age and MMSE scores in the four groups were performed using a Kruskal–Wallis test followed by a Dunn's multiple comparison test with a significance level of $p<0.05$. Correlations between the MMSE score and BF-227 retention in the neocortex or the cerebral atrophy index were examined using a non-parametric Spearman's rank correlation analysis. Correlations between the brain atrophy index and BF-227 retention were determined using Pearson's correlations. A linear model was applied to the data to obtain a correlation coefficient and *p* value. These analyses were performed using GraphPad Prism5 software (GraphPad, San Diego, CA).

4. Results

In order to confirm the selective binding ability of BF-227 to Aβ deposits, neuropathological examination was initially performed using BF-227 staining of AD temporal brain sections. Senile plaques were selectively stained with BF-227 and the staining pattern coincided well with Aβ immunostaining in an adjacent section (Fig. 1). Strikingly, cored plaques were intensely stained with BF-227, indicating preferential BF-227 binding to dense Aβ fibrils. Next,

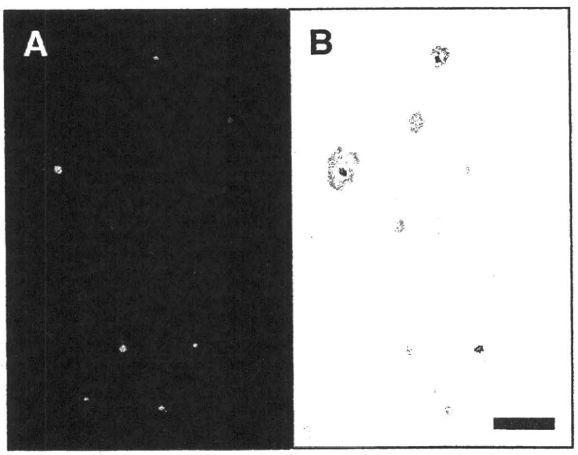

Fig. 1. (A) Neuropathological staining of human brain sections by BF-227. Amyloid plaques are clearly stained with BF-227 in AD temporal brain sections (B) BF-227 staining correlates well with Aβ immunostaining in adjacent sections. Scale bar = 100 μm.

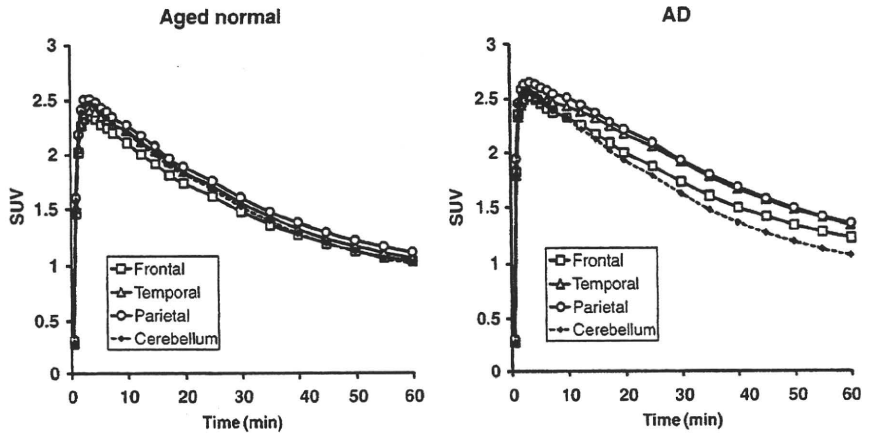

Fig. 2. Tissue time activity data for [^{11}C]BF-227-PET. SUV time activity curves of [^{11}C]BF-227 in the frontal cortex, lateral temporal cortex, parietal cortex and cerebellum are shown. Each point represents the mean of 12 control subjects (left) and 15 AD patients (right).

we performed clinical PET using [^{11}C]BF-227 in AD patients, MCI subjects and control subjects. The tissue time activity curves from [^{11}C]BF-227-PET in 15 AD patients and 12 normal controls are shown in Fig. 2. In AD patients, the frontal, temporal and parietal cortices retained [^{11}C]BF-227 to a greater extent at later time points, compared with controls. AD patients showed significantly higher SUVs in the temporal cortex and average neocortex than controls, but not in the cerebellum (Table 2). Therefore, neocortical SUV elevation in AD patients presumably reflects the specific binding of BF-227 to amyloid plaques. Representative images of [^{11}C]BF-227-PET and T1-weighted MRI in a normal control (70-year-old female, MMSE score 29), a MCI non-converter (76-year-old male, MMSE score 27), a MCI converter (85-year-old male, MMSE score 23), and an AD patient (62-year-old female, MMSE score 20) are shown in Fig. 3. Increased BF-227 retention was evident in both the MCI converter and the AD patient, but not in the control subject or the MCI non-converter. In AD patients, BF-227 SUVRs in the frontal, temporal, parietal and posterior cingulate cortices were significantly higher compared to the control subjects and the MCI non-converters (Table 2). A significant elevation of BF-227 SUVR was additionally observed in the frontal, temporal and parietal cortices of MCI converters compared with the control subjects. Consequently, the average neocortical SUVR was significantly higher in the AD patients and MCI converters than in normal subjects and MCI non-converters (Table 2). When a neocortical BF-227 SUVR of 1.11 (1.5SD above control mean) was used as a cut-off, sensitivity of 100% and a specificity of 91.7% in the discrimination between AD patients and normal subjects were achieved.

The voxel-based comparison of gray matter images using SPM5 demonstrated a significant decline of gray matter concentrations in the left ($-28, 14, -26, x, y, z$; $Z=5.26$) and the right ($32, 18, -26, x, y, z$; $Z=5.24$) medial temporal cortices of AD patients, compared with control subjects (Fig. 4A). SPM2 analysis using the same samples also showed a reduction of gray matter concentrations in nearly the same region and significance (data not shown). We drew the ROI in the parahippocampal area (Fig. 4B) and performed a comparison between the four groups. Significantly lower gray matter intensity was observed in the AD patients, MCI converters and MCI non-converters than in controls (Table 2, Fig. 5). However, age-related changes may be a confounding factor resulting in lower gray matter intensity in MCI groups, as MCI subjects were older than the normal control group. When a parahippocampal ROI value from SPM5 of 0.537 (2SD below control mean) was used as a cut-off, a sensitivity of 80.0% and a specificity of 100% were achieved in the discrimination between AD patients and normal subjects. No significant inter-group difference was observed in the percent global atrophy in VBM analysis due to substantial differences between individuals.

We focused on the comparison between the MCI converters and the non-converters, because these two populations showed no significant difference in age or MMSE scores. A significant inter-group difference was observed in the frontal and the average neocortical SUVR assayed by BF-227-PET, but not in the percent global atrophy or parahippocampal ROI value obtained by VBM-MRI (Table 2, Fig. 5). However, MCI converters showed a tendency toward lower parahippocampal ROI value derived from SPM5 than MCI non-converters.

Table 2
Summary of imaging measures.

	Normal	MCI non-converter	MCI converter	AD
BF-227 SUV in cerebellum	1.10 ± 0.19	1.08 ± 0.17	1.16 ± 0.22	1.16 ± 0.16
BF-227 SUV in frontal cortex	1.11 ± 0.19	1.10 ± 0.16	1.36 ± 0.33	1.31 ± 0.22
BF-227 SUV in temporal cortex	1.14 ± 0.19	1.19 ± 0.18	1.39 ± 0.28	1.45 ± 0.24[a]
BF-227 SUV in parietal cortex	1.20 ± 0.21	1.20 ± 0.18	1.38 ± 0.29	1.46 ± 0.23
BF-227 SUV in posterior cingulate cortex	1.22 ± 0.22	1.23 ± 0.22	1.39 ± 0.27	1.47 ± 0.21
Average neocortical BF-227 SUV	1.17 ± 0.20	1.18 ± 0.18	1.38 ± 0.29	1.42 ± 0.22[a]
BF-227 SUVR in frontal cortex	1.01 ± 0.06	1.02 ± 0.07	1.16 ± 0.10[a,b]	1.13 ± 0.08[a,b]
BF-227 SUVR in temporal cortex	1.04 ± 0.04	1.10 ± 0.07	1.20 ± 0.07[a]	1.24 ± 0.08[a,b]
BF-227 SUVR in parietal cortex	1.09 ± 0.04	1.12 ± 0.05	1.18 ± 0.07[a]	1.25 ± 0.08[a,b]
BF-227 SUVR in posterior cingulate cortex	1.11 ± 0.06	1.14 ± 0.07	1.20 ± 0.09	1.26 ± 0.05[a,b]
Average neocortical BF-227 SUVR	1.06 ± 0.04	1.09 ± 0.06	1.19 ± 0.07[a,b]	1.22 ± 0.06[a,b]
Percent global atrophy in VBM-MRI	4.24 ± 3.49	7.35 ± 5.94	5.96 ± 3.06	8.53 ± 4.44
Parahippocampal ROI value in VBM-MRI (SPM2)	0.642 ± 0.034	0.569 ± 0.039[a]	0.553 ± 0.044[a]	0.541 ± 0.055[a]
Parahippocampal ROI value in VBM-MRI (SPM5)	0.605 ± 0.034	0.510 ± 0.051[a]	0.473 ± 0.060[a]	0.475 ± 0.068[a]

[a] $p<0.05$ vs. aged normal.
[b] $p<0.05$ vs. MCI non-converter.

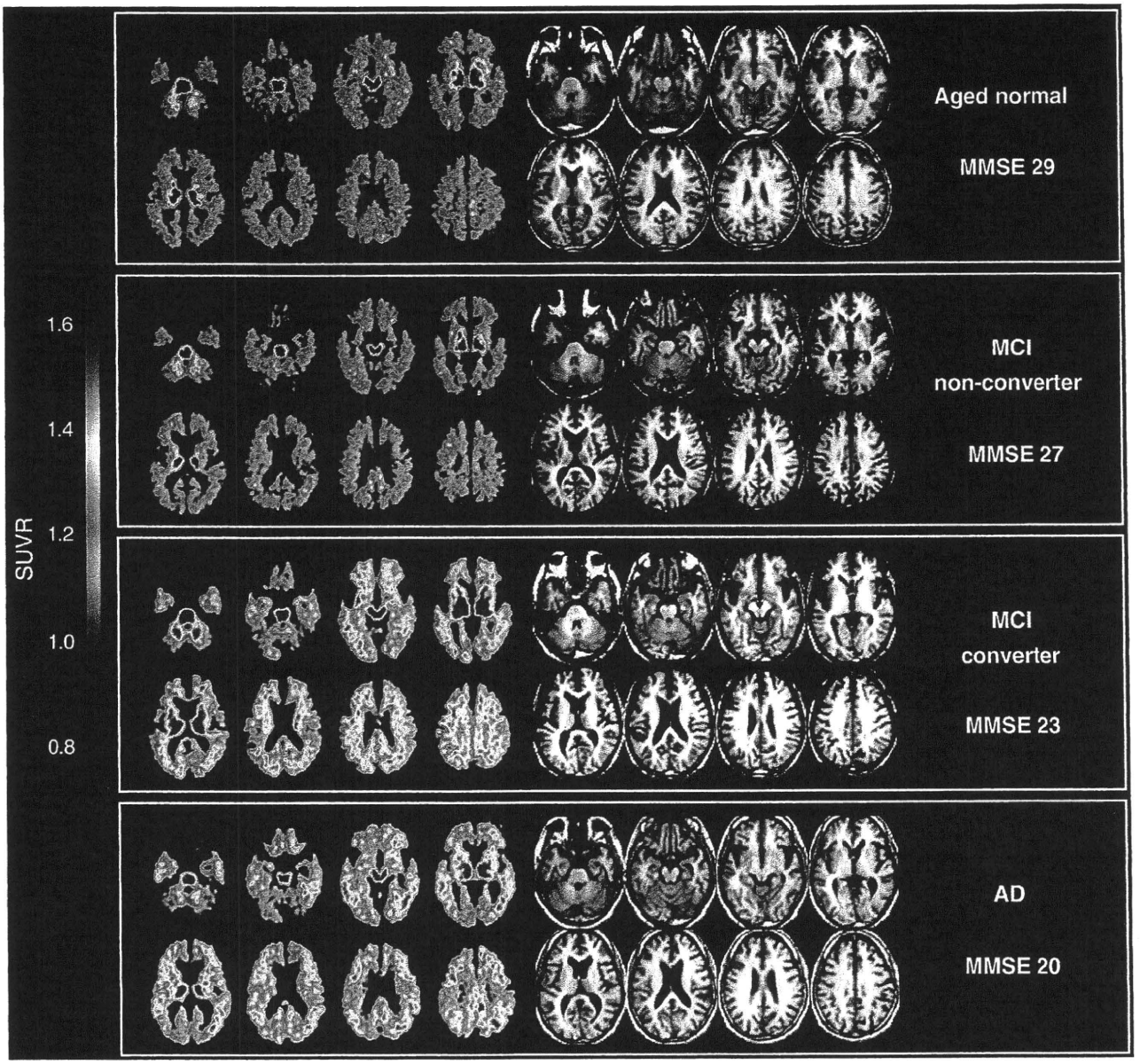

Fig. 3. Representative images of [^{11}C]BF-227–PET SUVR between 20 and 40 min post-injection (left) and T1-weighted MRI (right) in a control subject, a MCI non-converter, a MCI converter and an AD subject. The degree of [^{11}C]BF-227 retention is shown by color intensity from yellow to red in the cortex.

When we used a neocortical BF-227 SUVR of 1.11 as a cut-off, we achieved a sensitivity of 100% and a specificity of 71.4% in the discrimination between MCI converters and the MCI non-converters. These values were superior to the results of the parahippocampal ROI value derived from SPM5 (cut-off value: 0.537), which showed a sensitivity of 83.3% and a specificity of 42.9%. These data suggest that BF-227–PET is a better predictor of conversion from MCI to AD than VBM–MRI.

Next, we examined the correlations between MMSE scores and the three volume measurements (Fig. 6). When all subjects ($N=40$) were included in this analysis, a significant negative correlation was observed in all three measurements (BF-227 SUVR $r=-0.740$, $p<0.001$; percent global atrophy $r=-0.491$, $p=0.001$; parahippocampal ROI from SPM2 $r=0.674$, $p<0.001$; and parahippocampal ROI from SPM5 $r=0.687$, $p<0.001$). However, when we confined the analysis to the combined group of AD patients and MCI converters, we observed a significant correlation only between the percent global atrophy and the MMSE score (Spearman $r=-0.459$, $p=0.036$). In contrast, no significant correlation was observed between the parahippocampal ROI from SPM2 and the MMSE (Spearman $r=0.192$), between the parahippocampal ROI from SPM5 and the MMSE (Spearman $r=0.181$) or between the BF-227 SUVR in the neocortex and the MMSE (Spearman $r=-0.200$). Finally, no significant correlation was observed between the BF-227 SUVR and the percent global atrophy or parahippocampal atrophy in the analysis of all subjects.

5. Discussion

In the present study, MCI converters were more clearly distinguished from MCI non-converters by BF-227–PET than by VBM–MRI. The MCI non-converters showed a normal distribution of BF-227 except for one case, but also showed lower gray matter density in the parahippocampal gyrus than did normal controls. As a result, BF-227–PET achieved higher sensitivity and specificity in the discrimination between MCI converters and MCI non-converters than did VBM–MRI.

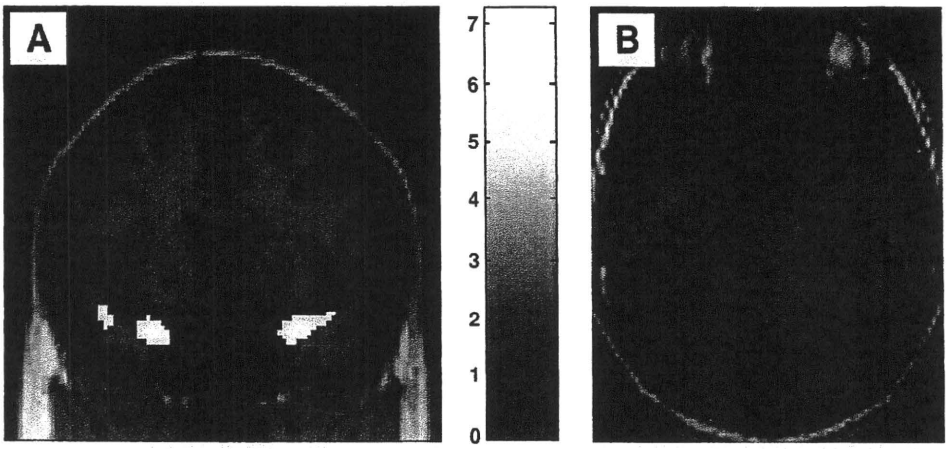

Fig. 4. (A) Areas of reduction in gray matter density of AD patients compared with aged normal controls. $p<0.05$, corrected for multiple comparisons. Left in the image is left in the brain. Color bars represent T values. (B) Regions of interest within the parahippocampal gyrus.

Our results strongly suggest that amyloid imaging using BF-227–PET will be a useful tool to predict conversion from MCI to AD, as previously shown for PIB–PET. [17,18] However, cerebral gray matter loss as determined by VBM–MRI was better correlated with the clinical severity of AD than BF-227–PET. Used together, BF-227–PET and VBM–MRI could be an effective method for the early diagnosis and severity tracking of AD. Our findings may be compatible with the theory that amyloid deposition reaches equilibrium or plateaus at an early stage of AD, making in vivo amyloid imaging useful in the examination of pre-symptomatic subjects [15,16]. Aβ deposition is a pathological hallmark of AD, but may also occur in normal elderly individuals who do not exhibit apparent cognitive decline. In fact, a PIB–PET study showed that 22% of healthy elderly individuals showed increased cortical PIB binding, indicating the presence of Aβ plaques in these non-symptomatic subjects [15]. A strong relationship between the impairment of episodic memory and PIB binding has also been shown both in subjects with MCI and in the normal population, suggesting that individuals with increased cortical PIB

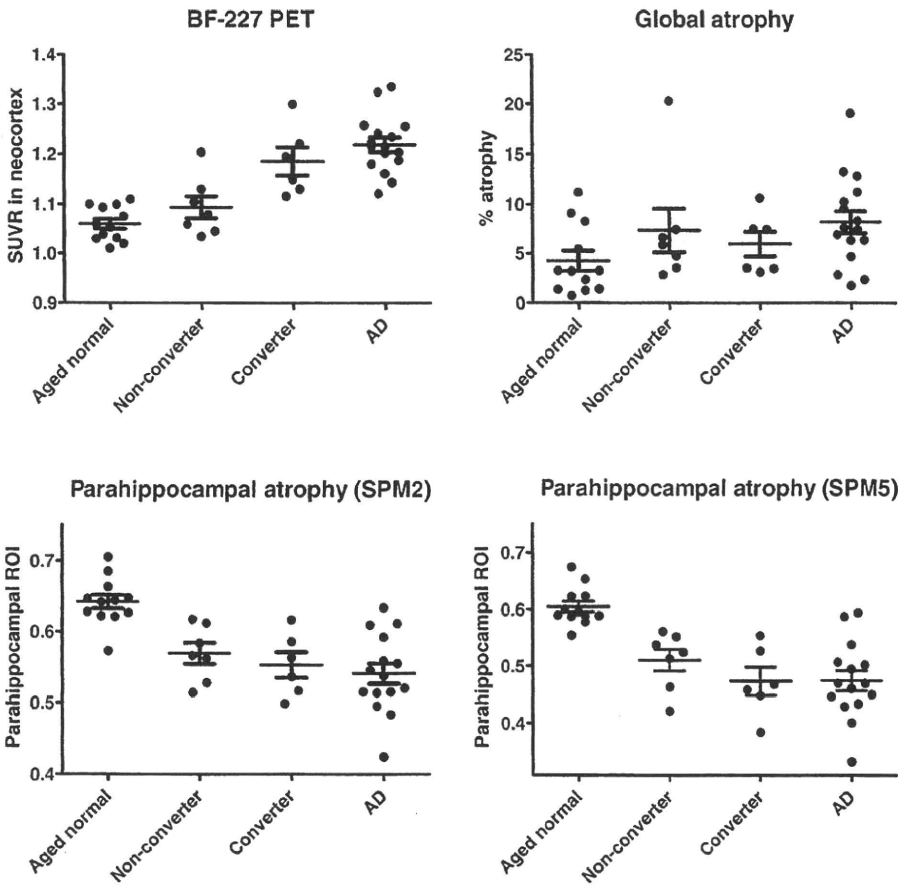

Fig. 5. Comparison of BF-227 SUVR in the neocortex (upper left), the percent global atrophy (upper right), the parahippocampal region of interest (ROI) value from gray matter images processed by SPM2 (lower left) and the parahippocampal ROI value from gray matter images processed by SPM5 (lower right) in control subjects, MCI non-converters, converters and AD patients.